



HAL
open science

TPLATE complex-dependent endocytosis attenuates CLAVATA1 signaling for shoot apical meristem maintenance

Jie Wang, Qihang Jiang, Roman Pleskot, Peter Grones, Elmehdi Bahafid,
Grégoire Denay, Carlos Galván-Ampudia, Xiangyu Xu, Michael Vandorpe,
Evelien Mylle, et al.

► **To cite this version:**

Jie Wang, Qihang Jiang, Roman Pleskot, Peter Grones, Elmehdi Bahafid, et al.. TPLATE complex-dependent endocytosis attenuates CLAVATA1 signaling for shoot apical meristem maintenance. EMBO Reports, 2023, 24 (9), pp.e54709. 10.15252/embr.202254709 . hal-04237830

HAL Id: hal-04237830

<https://hal.science/hal-04237830v1>

Submitted on 11 Oct 2023

HAL is a multi-disciplinary open access archive for the deposit and dissemination of scientific research documents, whether they are published or not. The documents may come from teaching and research institutions in France or abroad, or from public or private research centers.

L'archive ouverte pluridisciplinaire **HAL**, est destinée au dépôt et à la diffusion de documents scientifiques de niveau recherche, publiés ou non, émanant des établissements d'enseignement et de recherche français ou étrangers, des laboratoires publics ou privés.

1 TPLATE complex-dependent endocytosis attenuates CLAVATA1 signaling for shoot apical
2 meristem maintenance

3 Jie Wang^{1,2,3}, Qihang Jiang^{1,2}, Roman Pleskot^{1,2,4}, Peter Grones^{1,2}, Elmehti
4 Bahafid^{5,6}, Grégoire Denay^{5,6}, Carlos Galván-Ampudia⁷, , Xiangyu Xu^{1,2}, Michael
5 Vandorpe^{1,2}, Evelien Mylle^{1,2}, Ive De Smet^{1,2}, Teva Vernoux⁷, Rüdiger Simon^{5,6}, Moritz
6 K. Nowack^{1,2}, Daniel Van Damme^{1,2,*}

7 ¹Ghent University, Department of Plant Biotechnology and Bioinformatics,
8 Technologiepark 71, 9052 Ghent, Belgium

9 ²VIB Center for Plant Systems Biology, Technologiepark 71, 9052 Ghent, Belgium

10 ³Tobacco Research Institute, Chinese Academy of Agricultural Sciences, Qingdao,
11 Shandong 266101, China.

12 ⁴Institute of Experimental Botany, Czech Academy of Sciences, 165 02 Prague, Czech
13 Republic

14 ⁵Institute for Developmental Genetics, Heinrich-Heine University, University Street 1, D-
15 40225 Düsseldorf, Germany

16 ⁶Cluster of Excellence on Plant Sciences (CEPLAS), University Street 1, D-40225
17 Düsseldorf, German

18 ⁷Laboratoire Reproduction et Développement des Plantes, Univ Lyon, ENS de Lyon,
19 CNRS, INRAE, France

20 *Correspondence: daniel.vandamme@psb.vib-ugent.be (D.V.D.)

21

22

23

24

25

26

27

28

29 **Abstract**

30 Endocytosis regulates the turnover of cell surface localized receptors, which are crucial
31 for plants to rapidly respond to stimuli. The evolutionary ancient TPLATE complex (TPC)
32 plays an essential role in endocytosis in Arabidopsis plants. Knockout or knockdown of
33 single TPC subunits causes male sterility and seedling lethality phenotypes,
34 complicating analysis of the roles of TPC during plant development. Partially functional
35 alleles of TPC subunits however only cause mild developmental deviations. Here, we
36 took advantage of the partially functional TPLATE allele, WDXM2, to investigate a role
37 for TPC-dependent endocytosis in receptor-mediated signalling. We discovered that
38 reduced TPC-dependent endocytosis confers a hypersensitivity to very low doses of
39 CLAVATA3 peptide signalling. This hypersensitivity correlated with the abundance of
40 the CLAVATA3 receptor protein kinase CLAVATA1 at the plasma membrane. Genetic
41 and biochemical analysis as well as live-cell imaging revealed that TPC-dependent
42 regulation of CLAVATA3-dependent internalization of CLAVATA1 from the plasma
43 membrane is required for shoot stem cell homeostasis. Our findings provide evidence
44 that clathrin-mediated endocytosis and degradation of CLAVATA1 is a mechanism to
45 dampen CLAVATA3-mediated signaling during plant development.

46

47 **Key Words:** Clathrin-mediated endocytosis, TPLATE complex, CLAVATA3-
48 CLAVATA1 signaling, shoot apical meristem maintenance

49

50

51

52

53

54

55

56

57

58

59 Introduction

60 Coordinating cellular responses to environmental stimuli largely relies on receptor-like
61 kinases (RLKs) or receptor-like proteins (RLPs) localized on the plasma membrane
62 (PM), that are activated by cognate peptide ligands (Claus *et al*, 2018; Gou & Li, 2020;
63 Hohmann *et al*, 2017; Olsson *et al*, 2019). CLAVATA1(CLV1)-type receptors are one of
64 the most intensively studied groups of plant RLKs, and they are crucial for shoot apical
65 meristem (SAM) and root apical meristem (RAM) maintenance (Clark *et al*, 1993; Clark
66 *et al*, 1997; DeYoung *et al*, 2006; Deyoung & Clark, 2008; Dievart *et al*, 2003; Stahl
67 *et al*, 2013). PM abundance and vacuolar targeting of CLV1 depends on the CLAVATA3
68 (CLV3) peptide (Nimchuk *et al*, 2011). However, how CLV1 signaling is modulated by
69 its internalization remains unknown (Yamaguchi *et al*, 2016).

70 In plants, clathrin-mediated endocytosis (CME) is the best-characterized pathway by
71 which cells internalize transporters, receptors and their bound ligands from PM via
72 transport vesicles (Paez Valencia *et al*, 2016; Zhang *et al*, 2015). Internalization of PM
73 localized receptors can occur in a ligand-independent or ligand-dependent manner
74 (Beck *et al*, 2012; Ben Khaled *et al*, 2015; Irani *et al*, 2012; Mbengue M, 2016; Nimchuk
75 *et al.*, 2011; Ortiz-Morea *et al*, 2016) and serves either to attenuate signalling by
76 vacuolar degradation or to sustain signalling from endosomes (Claus *et al.*, 2018; Paez
77 Valencia *et al.*, 2016).

78 The heterotetrameric adaptor protein complex 2 (AP-2) and the octameric TPLATE
79 complex (TPC) jointly function as adaptor complexes to execute CME in plants (Di
80 Rubbo *et al*, 2013; Gadeyne *et al*, 2014; Zhang *et al.*, 2015). Knockout or strong
81 knockdown of single TPC subunits results in pollen and seedling lethality (Gadeyne *et al*,
82 *et al.*, 2014; Van Damme *et al*, 2006; Wang *et al*, 2019). Mild knockdown of TPC subunits
83 or destabilization of TPC by mutating the evolutionary most conserved domain (the
84 WDX domain) in the TPLATE subunit, however, results in viable plants, allowing to
85 address possible developmental functions for this complex (Bashline *et al*, 2015; Van
86 Damme *et al.*, 2006; Wang *et al*, 2021).

87 In this study, we took advantage of WDX domain-dependent TPC destabilization to
88 explore how reduced TPC-dependent endocytic capacity affects receptor-mediated
89 signaling in plants. We compared the response of control plants (*tplate*^{-/-}) rescued with
90 TPLATE-GFP) with that of plants expressing the partially functional allele (*tplate*^{-/-})
91 rescued with WDXM2-GFP) upon exposure to different types of exogenous peptides.

92 **Results and discussion**

93 **Reduced TPC-dependent endocytosis confers hypersensitivity to a subset of CLE**
94 **peptides**

95 *In vitro* bioassays comparing root growth in the presence or absence of exogenous
96 peptide ligands provide an easy readout and are widely employed to evaluate how
97 plants respond to peptide-dependent signaling (Anne *et al*, 2018; Blumke *et al*, 2021;
98 Breda *et al*, 2019; Graeff *et al*, 2020; Hazak *et al*, 2017; Hu *et al*, 2018; Poncini *et al*,
99 2017). To correlate peptide-dependent receptor signalling with CME capacity, we
100 selected several classes of peptide ligands. CME has been shown to internalize the
101 pattern recognition receptors PEP RECEPTOR1 (PEPR1) and FLAGELLIN SENSING 2
102 (FLS2), which are the respective receptors of the *Arabidopsis thaliana* endogenous
103 elicitor peptides (AtPEPs) and the bacterial peptide FLAGELLIN 22 (FLG22) (Mbengue
104 M, 2016; Ortiz-Morea *et al.*, 2016). We also included the C-TERMINALLY ENCODED
105 PEPTIDE 5 (CEP5), which impacts on primary root length and lateral root initiation via
106 its proposed receptor XYLEM INTERMIXED WITH PHLOEM 1 (XIP1)/CEP
107 RECEPTOR 1 (CEPR1) (Roberts *et al*, 2016). Finally, we included fourteen
108 CLV3/EMBRYO SURROUNDING REGION (CLE) peptides, which are essential for
109 shoot and root meristem maintenance by activating various plasma membrane-bound
110 receptors (Yamaguchi *et al.*, 2016).

111 TPLATE and WDXM2 rescued seedlings were grown in the presence of different CLE
112 peptides. The majority of the tested CLE peptides, which were applied at nanomolar
113 concentrations, elicited a similar response in WDXM2 and TPLATE seedlings (Fig
114 EV1A-B). However, we observed a strong hypersensitivity of WDXM2 seedlings to
115 CLV3, CLE10 and CLE40 (Fig EV1A-B). CLE40 is the closest homolog of CLV3 in
116 *Arabidopsis*, and both peptides are crucial for root and shoot meristem maintenance
117 (Brand *et al*, 2000; Clark *et al*, 1995; Fletcher *et al*, 1999; Hobe *et al*, 2003; Ito *et al*,
118 2006; Schlegel *et al*, 2021; Stahl *et al.*, 2013; Stahl *et al*, 2009; Yamaguchi *et al.*, 2016).
119 The specific hypersensitivity of the WDXM2 expressing seedlings to these two closely
120 related peptides hinted towards a connection between TPC-dependent endocytosis and
121 CLV1-type receptor signalling.

122 We subsequently treated TPLATE and WDXM2 rescued plants with CLV3, CLE40 at a
123 concentration of 10 nM as well as with different doses of FLG22, AtPEP1 and CEP5
124 peptides, previously shown to affect root growth (Poncini *et al.*, 2017), and we
125 compared the effect between our two backgrounds that differ in their endocytic capacity

126 (Wang *et al.*, 2021). After a 5-day exposure, both WDXM2 and TPLATE seedlings,
127 grown in the presence of the peptides, showed reduced root growth compared to the
128 control situation, indicating that they responded to the treatments. In contrast to the
129 clearly differential effect observed for CLV3 and CLE40 (Fig 1A-B), both backgrounds
130 responded similarly to FLG22 treatment and only a slight but statistically significant
131 difference was found in response to the low dose of AtPEP1 but not to the higher dose
132 (Fig 1C-D). We also did not observe any differential response between TPLATE and
133 WDXM2 rescued plants to both low and high doses of CEP5, although the latter
134 severely reduced root growth (Fig 1C-D). These results indicate that the differential
135 endocytic capacity between both backgrounds elicits hypersensitivity to CLE peptides,
136 but that the mild endocytic flux difference between both backgrounds is insufficient to
137 generate a differential developmental effect due to FLG22-, AtPEP1- or CEP5-
138 dependent receptor signaling at the concentrations used. We conclude that regulatory
139 mechanisms controlling the activity of those receptors remain sufficiently active in both
140 genetic backgrounds.

141 To independently confirm the observed hypersensitivity to CLV3 and CLE40, we tested
142 another genetic background affected in TPC function. The *twd40-2-3* mutant is a mild
143 knockdown allele of the TPC subunit TWD40-2 (Bashline *et al.*, 2015). Similar to our
144 partially functional WDXM2 allele, *twd40-2-3* mutant plants also exhibited a
145 hypersensitive response to low doses of CLV3 and CLE40 treatment (Fig EV2A-B).
146 Altogether, these results revealed that reduced TPC-dependent endocytosis enhances
147 CLV3 and CLE40 signalling in Arabidopsis roots.

148 **TPC-dependent endocytosis contributes to SAM maintenance through the** 149 **WUSCHEL signalling pathway**

150 Next to root meristem maintenance, CLV3-dependent signaling is also essential to
151 maintain SAM homeostasis. Long-term synthetic CLV3 peptide treatment dampens cell
152 proliferation and thus consumes SAM (Hu *et al.*, 2018; Ishida *et al.*, 2014). To
153 investigate the importance of TPC-dependent endocytosis for SAM maintenance, we
154 compared the sensitivity of TPLATE and WDXM2 rescued plants to long-term CLV3
155 peptide treatment. Seedling morphologies indicated that TPLATE and WDXM2
156 seedlings were equally capable of maintaining their SAM in the presence of very low
157 doses of exogenous CLV3 peptides (10 nM), even during long-term treatment (Fig 2A-
158 B). However, higher concentrations (100 nM and 1 μ M) of CLV3 revealed
159 hypersensitivity of WDXM2 seedlings and increasingly caused SAM termination in

160 independent mutant WDXM2 lines (Fig 2A-B and Fig EV3A-B). The hypersensitivity of
161 WDXM2 plants to CLV3 further correlated with the protein levels of the
162 complementation constructs in the rescued *tplate* mutant lines (Fig EV3C). These
163 results suggest that TPC-dependent endocytic deficiency causes a dose-dependent
164 hypersensitivity to CLV3-dependent receptor signalling.

165 In the SAM, CLV3 signalling functions in a negative feedback circuit to dampen stem
166 cell proliferation by regulating the expression of the homeodomain transcription factor
167 WUSCHEL (WUS) (Hazak & Hardtke, 2016; Kitagawa & Jackson, 2019; Yamaguchi *et*
168 *al.*, 2016). To further examine whether TPC-dependent endocytosis is involved in the
169 CLV–WUS feedback loop to regulate SAM homeostasis, we analyzed the expression
170 patterns of *WUS* in TPLATE and WDXM2 rescued plants following a three-day CLV3
171 peptide treatment. Both 10 nM and 100 nM CLV3 peptide treatment did not visibly
172 impair *WUS* promoter activity in TPLATE vegetative SAMs at the seedling level
173 compared to control conditions as visualized by GUS staining (Fig 2C-D). In WDXM2
174 vegetative SAMs, however, CLV3 application dampened *WUS* expression in a dose-
175 dependent manner (Fig 2C-D), which is coherent with the terminated SAM phenotype
176 observed at the rosette stage level upon prolonged treatment (Fig 2A-B). These
177 findings reveal that TPC-dependent endocytosis is involved in the regulation of CLV3-
178 *WUS* signaling in the SAM.

179 **TPC-dependent endocytosis internalizes CLV1 to dampen CLV3-dependent** 180 **signalling**

181 The receptor kinase CLV1 signals in response to CLV3 and plays a central role in shoot
182 meristem maintenance (Brand *et al.*, 2000; Clark *et al.*, 1997; Fletcher *et al.*, 1999;
183 Ogawa *et al.*, 2008; Shinohara & Matsubayashi, 2015; Somssich *et al.*, 2015). CLV1
184 levels increase at PM in the absence of CLV3 and accumulate in the vacuole in the
185 presence of CLV3 (Nimchuk *et al.*, 2011). CLV3-induced vacuolar accumulation of
186 CLV1 suggests a negative regulation of CLV3/CLV1 signaling by internalization, yet this
187 hypothesis remains to be experimentally tested (Yamaguchi *et al.*, 2016).

188 To characterize whether TPC-dependent endocytosis functions in CLV1 internalization,
189 we evaluated whether the response of TPLATE and WDXM2 rescued plants to CLV3
190 treatment depended on the presence of CLV1. Combining the *clv1-101* null allele
191 (Kinoshita A, 2010) with our TPLATE and WDXM2 rescued plants largely suppressed
192 the hypersensitivity to exogenous CLV3 leading to SAM termination in WDXM2,
193 although not completely (Fig 3A-B). Combining the strong and dominant-negative *clv1*

194 mutant allele *clv1-8* (Clark *et al.*, 1997; Dievart *et al.*, 2003) restored SAM maintenance
195 in WDXM2 in the presence of 100nM CLV3 (Fig 3A-B). The differential effect of
196 exogenous CLV3 on SAM activity between WDXM2, WDXM2/*clv1-101* and
197 WDXM2/*clv1-8* was also apparent in the number of leaves that the plants produced (Fig
198 3C).

199 These results reveal that CLV1 predominantly contributes to the hypersensitivity of
200 CLV3-dependent signalling in WDXM2 mutant plants. The different capacity of the *clv1-101*
201 null allele and the *clv1-8* dominant negative allele to reduce the sensitivity of
202 WDXM2 to CLV3 is likely attributed to genetic redundancy within the CLV1 receptor
203 family (DeYoung *et al.*, 2006; Deyoung & Clark, 2008; Nimchuk, 2017; Nimchuk *et al.*,
204 2015; Shinohara & Matsubayashi, 2015).

205 The WDXM mutation destabilizes TPC and thereby negatively affects endocytic
206 capacity (Wang *et al.*, 2021). The entire TPC complex is required to execute CME at
207 PM (Gadeyne *et al.*, 2014; Johnson *et al.*, 2021; Wang *et al.*, 2020; Wang *et al.*, 2021;
208 Yperman *et al.*, 2021b) and destabilizing TPC in WDXM2 rescued plants impairs
209 endocytic capacity while it does not affect recruitment of the two AtEH/Pan1 subunits at
210 PM, which are involved in promoting autophagy (Wang *et al.*, 2021; Wang *et al.*, 2019).
211 It is therefore likely that the CLV1-dependent hypersensitivity to CLV3 is linked to
212 altered endocytosis of CLV1 in WDXM2. CLV1 is a master regulator of flower
213 development (Clark *et al.*, 1997; Schoof *et al.*, 2000). Both TPLATE and WDXM2 are
214 expressed in the inflorescence meristem at roughly similar levels although in these
215 tissues, WDXM2 appears to be slightly less PM-associated compared to TPLATE (Fig
216 EV4A). CLV1 undergoes CLV3-mediated degradation in inflorescence meristems upon
217 induction of CLV3 expression in the *clv3-2* mutant background (Nimchuk *et al.*, 2011).
218 We subsequently addressed whether we could visualize ligand-dependent degradation
219 of CLV1 in our background. Live cell imaging revealed a strong vacuolar accumulation
220 of CLV1-GFP in the inflorescence meristem of the control background (TPLATE_3)
221 upon short time treatment with exogenous CLV3 peptide as well as a clear increase in
222 vacuolar flux visualized by an increased ratio of free GFP over full length protein, which
223 is a proxy for degradation, in the presence of CLV3. Moreover, our live cell imaging and
224 biochemical analysis also showed that CLV1 degradation was dampened in
225 inflorescence meristems in the WDXM2_3 background (Fig EV4B and EV4C). In
226 agreement with reduced internalization and degradation of CLV1 in WDXM2
227 inflorescence meristems, our live imaging analysis in vegetative meristems clearly
228 showed increased levels of CLV1-GFP in WDXM2 rescued plants compared to control

229 plants (Fig 4).

230 In vegetative meristems and in the presence of endogenous levels of CLV3 however,
231 signal intensities of CLV1 varied before and after exogenous CLV3 application. Live cell
232 imaging of the same vegetative meristem before and after CLV3 addition (Fig EV5A) as
233 well as quantification of treated and untreated meristems however revealed that CLV1
234 levels significantly reduced upon long-term (present in the medium from germination
235 onward; Fig 4) or short-term (10 and 30 min; Fig EV5B-E) exogenous CLV3 application
236 in TPLATE seedlings, while this was not the case in WDXM2 seedlings (Fig 4; Fig
237 EV5B-E).

238 These results strongly correlate the endocytosis deficiency in WDXM2 with impaired
239 internalization of CLV1 in inflorescence and in vegetative meristems. Increased CLV1
240 levels at PM are also in accordance with the fact that WDXM2 rescued plants are
241 hypersensitive to CLV3 peptide treatment, which correlates with strongly reduced *WUS*
242 levels and therefore likely increased CLV1-mediated transcriptional repression (Fig 2
243 and Fig 3). Despite this hypersensitivity, vegetative SAMs in WDXM2 appear enlarged
244 compared to those in TPLATE control seedlings (Fig 4 and Fig EV5). How this relates
245 to the abundance of CLV1 at PM and to altered *WUS* levels remains to be determined.

246 To establish a direct link between CLV1 and TPC, we examined the interaction
247 between TPC and CLV1. TPC, visualized using an antibody against TPLATE,
248 specifically co-purified with CLV1 in Arabidopsis seedlings when CLV1-2xGFP was
249 used as bait (Fig 5A). Next, we aimed to confirm this interaction and to determine which
250 adaptor complex subunits were involved. Tyrosine motif-based cargo recognition
251 involves the medium subunit of the Adaptor protein 2 complex, AP-2M (Arora & Damme,
252 2021), whose counterpart in TPC is the TML subunit. Furthermore, TPLATE co-purified
253 with CLV1 (Fig 5A) and AtEH1/Pan1 was shown to interact with cargo (Yperman *et al*,
254 2021a). We therefore selected these proteins for ratiometric bimolecular fluorescence
255 complementation (rBiFC) in *N. benthamiana*. Similar to previous experiments, the
256 shaggy-like kinase BIN2 served as negative control (Arora *et al*, 2020). We could not
257 visualize interaction between CLV1 and TPLATE, TML or AP-2M in this system (Fig 5B-
258 C). Our confocal analysis, however, clearly linked CLV1 to the plant-specific TPC
259 subunit AtEH1/Pan1 (Gadeyne *et al.*, 2014; Hirst *et al*, 2014) in the presence and
260 absence of exogenous CLV3 peptide (Fig 5B-C). The interaction between CLV1 and
261 AtEH1/Pan1 was further assessed via yeast-two-hybrid (Y2H) using the cytoplasmic
262 part of CLV1 and the N-terminal part of AtEH1/Pan1 ending just after the second EH
263 domain (Yperman *et al.*, 2021b). In total, 24 independent double transformations,

264 combining CLV1 with AtEH1/Pan1, CLV1 with empty vector control or AtEH1/Pan1 with
265 empty vector control were compared, alongside 8 double transformations of the empty
266 vector control and the p53-SV40 positive control (Fig 5D-E). The results clearly show a
267 specific interaction between CLV1 and AtEH1/Pan1 (Fig 5D-E). Both rBiFC and Y2H
268 therefore clearly link the cytoplasmic part of CLV1 to the N-terminal part of AtEH1/Pan1.
269 The N-terminal located EH domains of AtEH1/Pan1 were previously also shown to be
270 involved in membrane recruitment of TPC as well as in the internalization of the
271 Secretory Carrier Membrane Protein 5 (SCAMP5) via its double NPF motif (Johnson *et*
272 *al.*, 2021; Yperman *et al.*, 2021a). CLV1, in contrast to SCAMP5, does however not
273 contain obvious NPF motifs. How CLV1 is recognized by AtEH1/Pan1 therefore
274 remains to be determined.

275 Taken together, our findings reveal that the hypersensitivity of WDXM2 rescued plants
276 to CLV3 is most likely a consequence of sustained signalling from the PM, which is
277 caused by impaired internalization of CLV1 due to reduced TPC-dependent
278 endocytosis. TPC-dependent endocytosis, therefore, serves to internalize CLV1 to
279 attenuate CLV3 signalling to prevent meristem termination. Our work thus identifies
280 CME as a mechanism to control the availability of CLV1 at the PM and to tune the
281 activity of the shoot stem cell niche during plant development.

282 **Materials and Methods**

283 ***Molecular cloning***

284 mSCARLET (Bindels *et al.*, 2017) was amplified with a stop codon from plasmid pEB2-
285 mSCARLET (Addgene,104006), introduced into pDONRP2R-P3 via a Gateway BP
286 reaction (Invitrogen) and confirmed by sequencing. To generate mSCARLET-fused
287 expression constructs of TPLATE and WDXM2, The pDONR221-TPLATE and
288 pDONR221-WDXM2 motif substituted entry clones (Wang *et al.*, 2021) were combined
289 with pHm34GW (Karimi *et al.*, 2007), pDONRP4-P1r-Lat52 (Van Damme *et al.*, 2006),
290 and pDONRP2R-P3-mSCARLET in triple gateway LR reactions (Invitrogen).

291 The pBiFCt-2in1 BiFC vectors, which allow quantification of the observed Bimolecular
292 YPF fluorescence complementation by measuring the ratio between the intensity of the
293 YPF signal for a specific pair of interacting proteins and the intensity of the
294 constitutively expressed RFP which is present on the backbone of the vector, were
295 used to generate CLV1 related rBiFC constructs (Grefen & Blatt, 2012). The CLV1
296 entry clone for rBiFC reactions was amplified from a published plasmid (Schlegel *et al.*,

297 2021), while TPLATE, TML, AtEH1/Pan1 and AP2M were obtained from previously
298 reported rBiFC experiments (Arora *et al.*, 2020; Liu *et al.*, 2020; Yperman *et al.*, 2021a).
299 Entry clones were assembled in an empty rBiFC destination vector (pBiFCt-2in1-CC,
300 Addgene 105114 or pBiFCt-2in1-NC, Addgene 105112) with a Gateway LR
301 recombination reaction and selected using LB containing spectinomycin and Xgall. The
302 final rBiFC vectors were checked by restriction digestion and sequencing of the
303 recombination borders. For Y2H, the N-terminal domain of AtEH1/Pan1 (AA 1-527) was
304 amplified using following primer pairs (AtEH1_1-527_GBD_F
305 GCCATGGAGGCCGAATTCCCAATGGCGGGTCAGAATCCTAACATGG and
306 AtEH1_1-527_GBD_R CTGCAGGTCGACGGATCCCCTTATGCAGAATATCCATT
307 ACCTAGGTGATTAGC) and cloned into the pGBKT7 vector (Clontech). The
308 cytoplasmic part of CLV1 (AA 671 to 980, corresponding to the end of the
309 transmembrane helix, from amino acids LAWKL to the end of the uniprot sequence
310 Q9SYQ8) was amplified using following primer pairs (CLV1_671-980_GAD_F
311 GAGGCCAGTGAATTCCACCCACTCG CCTGGAAACTAACCGCCTTC and
312 CLV1_671-980_GAD_R TCCCGTATCGATGCCC
313 ACCCTTAGAACGCGATCAAGTTCGCCACGG) and cloned into pGADT7 (Clontech).
314 Both vectors were generated via Gibson assembly following Smal-dependent
315 linearization of the vectors. Plasmids were verified using sequencing.

316 ***Arabidopsis transgenic lines and growth conditions***

317 All plant materials used in this research are in the Columbia-0 (Col-0) ecotype
318 background. Information on plant materials is listed in Table EV1. To generate the
319 mSCARLET fusions of transgenic lines, *tplate* heterozygous mutant plants were
320 identified by genotyping PCR and were transformed with expression constructs of
321 TPLATE and WDXM2 fused to mSCARLET under the control of LAT52 promoter as
322 described before (Van Damme *et al.*, 2006; Wang *et al.*, 2021; Yperman *et al.*, 2021b).
323 Primary transformants were selected with Hygromycin, and those carrying the *tplate* T-
324 DNA insertion were identified via genotyping PCR. The rescued lines in the T2
325 generation were further genotyped to identify homozygous *tplate* mutants (Wang *et al.*,
326 2021).

327 For all the crosses, the same reporter line or mutant plant was used as male to cross
328 with TPLATE and WDXM2 rescued lines respectively. The *pWUS::GUS* (Su *et al.*, 2009)
329 reporter line was crossed into TPLATE_1 and WDXM2_1 rescued mutant backgrounds.
330 In the progeny, F2 plants were genotyped to obtain homozygous *tplate* mutant

331 backgrounds. The F3 or F4 generation plants were screened to identify homozygous
332 plants for *pWUS::GUS* expression by GUS staining. The *clv1* null mutant *clv1-101*
333 (Kinoshita A, 2010) and the dominant-negative *clv1-8* mutant (Dievart *et al.*, 2003) were
334 crossed into the TPLATE_1 and WDXM2_1 rescued lines. The F2 or F3 generation
335 plants were genotyped or sequenced to identify the *tplate/clv1-101* or *tplate/clv1-8*
336 double mutant backgrounds. To introduce the CLV1 marker line into TPLATE and
337 WDXM2 rescued lines, a wild type Col-0 plant expressing the functional pCLV1::CLV1-
338 GFP (Schlegel *et al.*, 2021) was backcrossed to Col-0 and a single locus expression F2
339 line was identified by segregation using Basta (20 mg/L) selection. Then the F2 Basta
340 resistant CLV1-GFP expressing plant was used to cross with the TPLATE_3 and
341 WDXM2_3 rescued plants. In the progeny, plants homozygous for the *tplate* mutant
342 background were identified by genotyping PCR while homozygous expression of CLV1-
343 GFP was selected by segregation on BASTA. For co-IP experiments, the
344 pCLV1::CLV1-2xGFP line was used (Nimchuk *et al.*, 2011).

345 Seeds were sterilized by chlorine gas sterilization and sown on ½ MS medium plates
346 without sugar following a 3-day vernalization period at 4°C. Seedlings were grown in a
347 growth chamber under continuous light conditions at 21°C.

348 ***Phenotypic analysis***

349 Sequences of CLE peptides described before (Yamaguchi *et al.*, 2016) were ordered
350 from GeneScript. Information on the peptides is listed in Table EV2. For shoot
351 treatments, seedlings were grown horizontally on ½ MS medium supplemented with or
352 without the indicated concentration of CLV3 peptide for 3 weeks. Plants with terminated
353 shoots were counted manually. For root growth assays, seedlings were initially grown
354 on ½ MS medium supplemented with or without CLE peptides for a certain duration
355 (data depicted in Figure EV1). For the FLG22, AtPEP, CEB5, CLV3 and CLE40
356 peptides depicted in Figure 1 and in Figure 2, seedlings were grown on ½ MS plates
357 and then transferred to plates with and without the indicated amount of peptides. Plates
358 with seedlings were scanned and root lengths were measured with the Fiji software
359 package (<https://imagej.net/software/fiji/>) equipped with the NeuronJ plugin (Meijering *et al.*, 2004). Quantification of the number of leaves in Figure 3C was done manually using
360 the cell counter plugin in Fiji.
361

362 ***GUS staining***

363 GUS staining was performed as described before (Lammens *et al*, 2008). Seedlings (3-
364 days after putting the plates in continuous light, i.e. roughly one day after germination)
365 expressing *pWUS::GUS* grown on ½ MS with or without CLV3 peptide were harvested
366 and incubated with 80% cold acetone for 30 min. After that, seedlings were washed
367 with phosphate buffer (pH = 7.2), incubated in GUS staining solution (1 mg/ml of 5-
368 bromo-4-chromo-3-indolyl β-D-glucuronide, 2 mM ferricyanide, and 0.5 mM
369 ferrocyanide in 100 mM phosphate buffer pH 7.2) and kept at 37 °C in the dark for 3
370 hours. After GUS staining, seedlings were cleared with lactic acid and visualized
371 between slide and coverslip on a BX51 light microscope (Olympus) using a 10x or 20x
372 magnification.

373 ***Nicotiana benthamiana* infiltration**

374 Three- to four-week-old *Nicotiana benthamiana* plants grown in greenhouse under long-
375 day conditions (06-22 h light, 100 PAR, 21°C) were used for infiltration as described
376 before (Arora *et al.*, 2020). 3 days after infiltration, *N. benthamiana* leaves were imaged
377 with an SP8X confocal microscope. CLV3 peptide (1 μM) in infiltration buffer (10 mM
378 MgCl₂ and 10 mM MES, pH 5.6) was applied via leaf infiltration. After 5 min incubation,
379 the injected samples were imaged within 30 min.

380 **Live-Cell Imaging and Analysis**

381 A Leica SP8X confocal microscope equipped with a white laser was used for all
382 confocal imaging via a 40x (HC PL APO CS2, NA=1.10) water- immersion corrected
383 objective except the flower meristem imaging.

384 rBiFC images were acquired with Hybrid detectors (HyDTM) using a time-gated window
385 between 0.3 ns-6.0 ns and in line sequential mode. YFP signals were acquired using
386 WLL 514 nm excitation and an emission window of 520-550 nm, and RFP signals were
387 detected using WLL 561 nm excitation and an emission window of 580-650 nm. All
388 images were taken using the same settings for YFP and RFP detection and saturation
389 was avoided in order not to interfere with the ratiometric quantification.

390 For CLV1-GFP imaging in vegetative SAMs in Figure 4 and Figure EV5B-E, seeds
391 expressing CLV1-GFP in TPLATE and WDXM2 rescued mutant backgrounds were
392 germinated on ½ MS plates supplemented with or without 100 nM of CLV3 peptide.
393 Seedlings were imaged following 3-days after putting the plates in continuous light,
394 which roughly equals 1 day after germination. For CLV1-GFP imaging upon short-term

395 CLV3 peptide treatment in Figure EV5, seedlings grown on ½ MS plates (3 days in light)
396 were used. After removal of the cotyledons, seedlings were incubated in ½ MS medium
397 containing 1 µM CLV3 peptide and 0.1% Tween 20 (v/v) for 10 or 30 min, and washed
398 with water shortly 3 times. Prior to imaging, seedlings expressing CLV1-GFP were
399 stained with PI solution (10 µg/mL) for 1 to 2 min. The Hybrid detectors (HyDTM) were
400 employed to image PI (excitation at 561 nm, emission between 600-700 nm) and CLV1-
401 GFP (excitation at 488 nm, emission between 500-540 nm) without (PI) or with (GFP) a
402 time-gated window between 0.3 ns-6.0 ns. To achieve sufficient signal when imaging
403 CLV1-GFP in the vegetative SAMs of TPLATE-3 and WDXM2_3 seedlings,
404 accumulative imaging was used. Images were acquired using 8 times line accumulation
405 and 2 times frame averaging.

406 For the flower SAM imaging in Figure EV4A, Arabidopsis plants were grown in soil for 4
407 weeks at 21 °C under long day condition (16 h light : 8 h dark, LED 150 µmol/m²/s).
408 Primary inflorescence shoot apical meristems were dissected, mounted in ACM and
409 then stained with 100 µM propidium iodide (PI; Merck) for 5 min prior to imaging
410 (Brunoud *et al*, 2020). Meristems were imaged with a Zeiss LSM 710 spectral
411 microscope using the following settings: GFP (excitation at 488 nm, emission between
412 510-558 nm) and propidium iodide (excitation 488 nm, emission between 605-650 nm).

413 For CLV1-GFP imaging in vegetative SAMs in Figure EV5A, vegetative shoot apices at
414 3 DAG were manually dissected under a stereo microscope by removing the leaf
415 primordia. The cell wall was stained with propidium iodide (PI). After removal of the leaf
416 primordia, vegetative SAMs were treated with ½ MS medium containing 1 µM CLV3
417 peptide and 0.1% Tween 20 and imaged at 0 min and 30 min after treatment. Z-stacks
418 of vegetative SAMs were acquired using a Zeiss LSM 780 confocal microscope (40×
419 water immersion objective, Zeiss C-PlanApo, NA 1.2). GFP was excited with an Argon
420 laser at 488 nm and emission was detected using a 490-530 nm window. PI was
421 excited at 561 nm by a DPSS laser and detected using a 590-650 nm window.

422 For the flower SAM imaging in Figure EV4B, IFMs from the pCLV1:CLV1-GFP reporter
423 line were dipped for 1 minute into a peptide solution containing 100 µM CLV3 peptide,
424 0.1% DMSO, and 0.01% Silwet, and then incubated for 30 minutes before imaging. For
425 the mock treatment, IFMs were dipped for 1 minute into a solution containing 0.1%
426 DMSO and 0.01% Silwet, and then incubated for 30 minutes before imaging.

427 To image IFMs, inflorescences were cut off and fixed to double-sided adhesive tape on
428 an objective slide, and then dissected. The cell walls were stained with 5 mM PI for 2

429 minutes. Inflorescences were then washed three times with water and covered with a
430 cover slide before being placed under the microscope. All IFM imaging was acquired
431 using a Zeiss LSM 880 confocal microscope equipped with a 40× water immersion
432 objective (Zeiss C-PlanApo, NA 1.2). GFP was excited with an Argon laser at 488 nm,
433 and emission was detected using a 490-530 nm window. PI was excited at 561 nm by a
434 DPSS laser and detected using a 590-650 nm window.

435 The quantification of rBiFC and SAM images was performed using Fiji. For rBiFC, a
436 region of interest (ROI) on PM of the cells was selected and the intensities of YFP and
437 RFP signals were measured. The ratios between YFP and RFP signals per cell were
438 then calculated and plotted. For the quantification of CLV1-GFP in TPLATE and
439 WDXM2 vegetative SAMs, a region of interest (ROI) covering the meristem was defined
440 and the CLV1-GFP signal intensities were measured. Only images with less than 1%
441 saturated pixels were quantified. The histogram function in Fiji was used to generate
442 intensity values (8-bit gray values) for each pixel and the top 10% highest intensity
443 pixels were used to calculate the mean fluorescence intensities using an in-house
444 designed script in Microsoft Excel. Using a selection of the strongest intensity pixels for
445 the calculations omits background noise that otherwise reduces the average
446 fluorescence intensities of the quantifications and follows from the rationale that the
447 fluorescence is linked to the endomembrane system and therefore not continuously
448 present throughout the selected ROI. Similar approaches are also used to calculate
449 ratios of endocytic flux between PM and endosomal compartments (Dejonghe *et al*,
450 2016; Mishev *et al*, 2018).

451 ***Protein extraction and Western blotting***

452

453 Arabidopsis seedlings were grown for 5 days on ½ MS medium without sugar under
454 continuous light conditions. Seedlings were harvested, flash-frozen, and grinded in
455 liquid nitrogen. Proteins were extracted in a 1:1 ratio, buffer (ml):seedlings (g), in HB+
456 buffer, as described before (Van Leene *et al*, 2015). Protein extracts were incubated for
457 30 min at 4°C on a rotating wheel before spinning down twice at 20,000 g for 20 min.
458 The supernatant concentration was measured using the Bradford Protein Assay
459 (Invitrogen), and equal amounts of proteins were loaded on 4 to 20% gradient gels (Bio-
460 Rad). Gels were transferred to nitrocellulose membranes using the Trans-Blot Turbo
461 system (Bio-Rad). Blots were incubated with α-TPLATE appendage antibodies (rabbit)
462 (Dejonghe *et al*, 2019) and imaged on a ChemiDoc Imaging System (Bio-Rad).

463

464 **Co-immunoprecipitation**

465

466 For experiments performed on 5 days old seedlings, entire seedlings of Col-0,
467 pCLV1::CLV1-2xGFP and 35S::eGFP were ground to a fine powder using liquid
468 nitrogen. For experiments performed on inflorescence meristems of lines expressing
469 pCLV1::CLV1-GFP in TPLATE_3 and WDXM2_3 backgrounds, the inflorescence
470 meristems were dipped into a solution of 100 μ M CLV3 peptide and 0,01% Silwet L-77.
471 After 30 min, the flower meristems were harvested and ground to a fine powder using
472 liquid nitrogen. Finely ground material was suspended in homogenization extraction
473 buffer [150 mM Tris-HCl, 150 mM NaCl, 0.5 mM EDTA, 10% glycerol, 1 mM sodium
474 molybdate, 1 mM NaF, 10 mM DTT, 1% IGEPAL CA-630 (Sigma-Aldrich,USA) with
475 Complete Ultra EDTA-free Protease Inhibitor Cocktail Tablets (Roche, Switzerland; 1
476 tablet per 10 mL)]. After 30 min of rotation at 4 °C, cell debris was removed from the
477 samples by centrifugation for 15 min at 2000 g at 4 °C. Supernatant was transferred to a
478 new tube through Miracloth (Millipore Sigma, USA). Then, 50 μ L pre-equilibrated GFP-
479 Trap®_MA beads (ChromoTek, Germany) was added into each sample and samples
480 were incubated for 2 h at 4 °C to maximize the protein binding. Afterwards, the beads
481 were washed two times with wash buffer (20 mM Tris-HCl pH 7.5, 150 mM NaCl).
482 Protein was eluted from the beads by adding Laemmli sample buffer (Bio-rad,
483 Laboratories, Inc., USA), Sample Reducing Agent (Invitrogen, USA) and incubating at
484 70 °C for 10 min.

485

486 The proteins were separated on 4–15% SDS-PAGE stain-free protein gel (Bio-Rad
487 Laboratories, Inc., USA), followed by transferring onto a Trans-Blot® Turbo™ Mini
488 PVDF Transfer Packs (Bio-Rad Laboratories, Inc., USA). After blocking with 5% Skim
489 Milk (Difco,USA) for 1 h at room temperature, blots were incubated with α GFP-HRP
490 (ChromoTek, Germany) (1:2000) or α TPLATE2 (rabbit) (Dejonghe et al., 2019)
491 overnight at 4 °C. Imaging was done using Chemiluminescent substrate (Thermo Fisher
492 Scientific, USA) and detected by ChemiDoc™ MP Imaging System (Bio-Rad
493 Laboratories, Inc., USA).

494

495 The quantification of the band intensities on the WB from the CLV1 IP (Figure EV4C)
496 was performed using ImageJ, by marking the region of the band with an ROI and
497 measuring the mean signal intensity.

498

499 **Yeast two hybrid analysis**

500

501 The N-terminal part of AtEH1/Pan1 (AA 1-527) up to the coiled coil domain in pGBKT7
502 and the cytoplasmic part of CLV1 (AA 671-980) in pGADT7 were combined with each
503 other and with empty control plasmids using the Matchmaker™ Gold Yeast Two-Hybrid
504 System (Clontech). The vectors were co-transformed into the Y2Hgold MATa Yeast
505 strain. Auto-activation was tested by co-transforming each vector with the
506 corresponding empty pGADT7 and pGBKT7 vectors. The empty pGADT7 and pGBKT7
507 were also co-transformed as a negative control and as a positive control, we used the
508 pGADT7-SV40 T-Ag and pGBKT7-p53 supplied with the Matchmaker system
509 (Clontech).

510 Colonies of double transformed yeasts were first selected on SD -Leu -Trp plates. After
511 3 days at 30 °C, colonies were picked and grown for 3 days in liquid -Leu -Trp medium
512 at 30 °C 200 rpm. Fully grown cultures were diluted 1/5 in -L-T-H and 10 µl was spotted
513 on SD -Leu -Trp and SD -Leu -Trp -His plates. Pictures were taken after 3 days at
514 30 °C.

515

516 **Statistical analysis**

517 The R package in R studio (www.rstudio.com) was used. Data were tested for normality
518 and heteroscedasticity, after which the multcomp package was used (Herberich *et al*,
519 2010).

520

521 **Data availability**

522 This study includes no data deposited in external repositories. Data used for
523 quantifications as well as full Western blots can be found in the source data file. All
524 material will be made available upon reasonable request to the corresponding author
525 (daniel.vandamme@psb.vib-ugent.be).

526

527 **Acknowledgements**

528 We would like to thank Elliot Meyerowitz, Marcus Heisler and Thomas Laux for
529 constructive discussions. This work was supported by the European Research Council,
530 Grant 682436 to D.V.D.; the Research Foundation–Flanders, Grant 1226420N to P.G.;
531 The China Scholarship Council, grant 201508440249 to J.W.; grant 201906760018 to
532 Q.J. and grant 201706350153 to X.X.; Ghent University Special Research co-funding,

533 grant ST01511051 to J.W and the DFG, grant CRC1208 to R.S.

534

535 **Disclosure and competing interests statements**

536 The authors declare that they have no conflict of interest.

537

538 **References**

- 539 Anne P, Amiguet-Vercher A, Brandt B, Kalmbach L, Geldner N, Hothorn M, Hardtke CS (2018)
540 CLERK is a novel receptor kinase required for sensing of root-active CLE peptides in
541 Arabidopsis. *Development* 145: 1-10
- 542 Arora D, Abel NB, Liu C, Van Damme P, Yperman K, Eeckhout D, Vu LD, Wang J, Tornkvist A,
543 Impens F *et al* (2020) Establishment of Proximity-Dependent Biotinylation Approaches in
544 Different Plant Model Systems. *Plant Cell* 32: 3388-3407
- 545 Arora D, Damme DV (2021) Motif-based endomembrane trafficking. *Plant Physiol* 186: 221-238
- 546 Bashline L, Li S, Zhu X, Gu Y (2015) The TWD40-2 protein and the AP2 complex cooperate in
547 the clathrin-mediated endocytosis of cellulose synthase to regulate cellulose biosynthesis. *Proc*
548 *Natl Acad Sci U S A* 112: 12870-12875
- 549 Beck M, Zhou J, Faulkner C, MacLean D, Robatzek S (2012) Spatio-temporal cellular dynamics
550 of the Arabidopsis flagellin receptor reveal activation status-dependent endosomal sorting. *Plant*
551 *Cell* 24: 4205-4219
- 552 Ben Khaled S, Postma J, Robatzek S (2015) A moving view: subcellular trafficking processes in
553 pattern recognition receptor-triggered plant immunity. *Annu Rev Phytopathol* 53: 379-402
- 554 Bindels DS, Haarbosch L, van Weeren L, Postma M, Wiese KE, Mastop M, Aumonier S,
555 Gotthard G, Royant A, Hink MA *et al* (2017) mScarlet: a bright monomeric red fluorescent
556 protein for cellular imaging. *Nat Methods* 14: 53-56
- 557 Blumke P, Schlegel J, Gonzalez-Ferrer C, Becher S, Pinto KG, Monaghan J, Simon R (2021)
558 Receptor-like cytoplasmic kinase MAZZA mediates developmental processes with CLAVATA1
559 family receptors in Arabidopsis. *J Exp Bot* 72: 4853-4870
- 560 Brand U, Fletcher JC, Hobe M, Meyerowitz EM, Simon R (2000) Dependence of stem cell fate in
561 Arabidopsis on a feedback loop regulated by CLV3 activity. *Science* 289: 617-619
- 562 Breda AS, Hazak O, Schultz P, Anne P, Graeff M, Simon R, Hardtke CS (2019) A Cellular
563 Insulator against CLE45 Peptide Signaling. *Curr Biol* 29: 2501-2508.e3
- 564 Brunoud G, Galvan-Ampudia CS, Vernoux T (2020) Methods to Visualize Auxin and Cytokinin
565 Signaling Activity in the Shoot Apical Meristem. *Methods Mol Biol* 2094: 79-89
- 566 Clark SE, Running MP, Meyerowitz EM (1993) CLAVATA1, a regulator of meristem and flower
567 development in Arabidopsis. *Development* 119: 397-418
- 568 Clark SE, Running MP, Meyerowitz EM (1995) Clavata3 Is a Specific Regulator of Shoot and
569 Floral Meristem Development Affecting the Same Processes as Clavata1. *Development* 121:
570 2057-2067
- 571 Clark SE, Williams RW, Meyerowitz EM (1997) The CLAVATA1 gene encodes a putative
572 receptor kinase that controls shoot and floral meristem size in Arabidopsis. *Cell* 89: 575-585
- 573 Claus LAN, Savatin DV, Russinova E (2018) The crossroads of receptor-mediated signaling and
574 endocytosis in plants. *J Integr Plant Biol* 60: 827-840
- 575 Dejonghe W, Kuenen S, Mylle E, Vasileva M, Keech O, Viotti C, Swerts J, Fendrych M, Ortiz-
576 Morea FA, Mishev K *et al* (2016) Mitochondrial uncouplers inhibit clathrin-mediated endocytosis
577 largely through cytoplasmic acidification. *Nat Commun* 7: 11710
- 578 Dejonghe W, Sharma I, Denoo B, De Munck S, Lu Q, Mishev K, Bulut H, Mylle E, De Rycke R,
579 Vasileva M *et al* (2019) Disruption of endocytosis through chemical inhibition of clathrin heavy
580 chain function. *Nat Chem Biol* 15: 641-649
- 581 DeYoung BJ, Bickle KL, Schrage KJ, Muskett P, Patel K, Clark SE (2006) The CLAVATA1-
582 related BAM1, BAM2 and BAM3 receptor kinase-like proteins are required for meristem function
583 in Arabidopsis. *Plant J* 45: 1-16

584 Deyoung BJ, Clark SE (2008) BAM receptors regulate stem cell specification and organ
585 development through complex interactions with CLAVATA signaling. *Genetics* 180: 895-904
586 Di Rubbo S, Irani NG, Kim SY, Xu ZY, Gadeyne A, Dejonghe W, Vanhoutte I, Persiau G,
587 Eeckhout D, Simon S *et al* (2013) The clathrin adaptor complex AP-2 mediates endocytosis of
588 brassinosteroid insensitive1 in Arabidopsis. *Plant Cell* 25: 2986-2997
589 Dievart A, Dalal M, Tax FE, Lacey AD, Huttly A, Li J, Clark SE (2003) CLAVATA1 dominant-
590 negative alleles reveal functional overlap between multiple receptor kinases that regulate
591 meristem and organ development. *Plant Cell* 15: 1198-1211
592 Fletcher JC, Brand U, Running MP, Simon R, Meyerowitz EM (1999) Signaling of cell fate
593 decisions by CLAVATA3 in Arabidopsis shoot meristems. *Science* 283: 1911-1914
594 Gadeyne A, Sanchez-Rodriguez C, Vanneste S, Di Rubbo S, Zauber H, Vanneste K, Van Leene
595 J, De Winne N, Eeckhout D, Persiau G *et al* (2014) The TPLATE adaptor complex drives
596 clathrin-mediated endocytosis in plants. *Cell* 156: 691-704
597 Gou X, Li J (2020) Paired Receptor and Coreceptor Kinases Perceive Extracellular Signals to
598 Control Plant Development. *Plant Physiol* 182: 1667-1681
599 Graeff M, Rana S, Marhava P, Moret B, Hardtke CS (2020) Local and Systemic Effects of
600 Brassinosteroid Perception in Developing Phloem. *Curr Biol* 30: 1626-1638.e1623
601 Grefen C, Blatt MR (2012) A 2in1 cloning system enables ratiometric bimolecular fluorescence
602 complementation (rBiFC). *Biotechniques* 53: 311-314
603 Hazak O, Brandt B, Cattaneo P, Santiago J, Rodriguez-Villalon A, Hothorn M, Hardtke CS (2017)
604 Perception of root-active CLE peptides requires CORYNE function in the phloem vasculature.
605 *EMBO Rep* 18: 1367-1381
606 Hazak O, Hardtke CS (2016) CLAVATA 1-type receptors in plant development. *J Exp Bot* 67:
607 4827-4833
608 Herberich E, Sikorski J, Hothorn T (2010) A robust procedure for comparing multiple means
609 under heteroscedasticity in unbalanced designs. *PLoS ONE* 5: e9788
610 Hirst J, Schlacht A, Norcott JP, Traynor D, Bloomfield G, Antrobus R, Kay RR, Dacks JB,
611 Robinson MS (2014) Characterization of TSET, an ancient and widespread membrane
612 trafficking complex. *eLife* 3: e02866
613 Hobe M, Muller R, Grunewald M, Brand U, Simon R (2003) Loss of CLE40, a protein functionally
614 equivalent to the stem cell restricting signal CLV3, enhances root waving in Arabidopsis. *Dev*
615 *Genes Evol* 213: 371-381
616 Hohmann U, Lau K, Hothorn M (2017) The Structural Basis of Ligand Perception and Signal
617 Activation by Receptor Kinases. *Annu Rev Plant Biol* 68: 109-137
618 Hu C, Zhu Y, Cui Y, Cheng K, Liang W, Wei Z, Zhu M, Yin H, Zeng L, Xiao Y *et al* (2018) A
619 group of receptor kinases are essential for CLAVATA signalling to maintain stem cell
620 homeostasis. *Nat Plants* 4: 205-211
621 Irani NG, Di Rubbo S, Mylle E, Van den Begin J, Schneider-Pizon J, Hnilikova J, Sisa M, Buyst
622 D, Vilarrasa-Blasi J, Szatmari AM *et al* (2012) Fluorescent castasterone reveals BRI1 signaling
623 from the plasma membrane. *Nat Chem Biol* 8: 583-589
624 Ishida T, Tabata R, Yamada M, Aida M, Mitsumasu K, Fujiwara M, Yamaguchi K, Shigenobu S,
625 Higuchi M, Tsuji H *et al* (2014) Heterotrimeric G proteins control stem cell proliferation through
626 CLAVATA signaling in Arabidopsis. *EMBO Rep* 15: 1202-1209
627 Ito Y, Nakanomyo I, Motose H, Iwamoto K, Sawa S, Dohmae N, Fukuda H (2006) Dodeca-CLE
628 peptides as suppressors of plant stem cell differentiation. *Science* 313: 842-845
629 Johnson A, Dahhan DA, Gnyliukh N, Kaufmann WA, Zheden V, Costanzo T, Mahou P, Hrtyan M,
630 Wang J, Aguilera-Servin J *et al* (2021) The TPLATE complex mediates membrane bending
631 during plant clathrin-mediated endocytosis. *Proc Natl Acad Sci U S A* 118: e2113046118
632 Karimi M, Depicker A, Hilson P (2007) Recombinational cloning with plant gateway vectors.
633 *Plant Physiol* 145: 1144-1154
634 Kinoshita A BS, Osakabe Y, Mizuno S, Nagawa S, Stahl Y, Simon R, Yamaguchi-Shinozaki K,
635 Fukuda H, Sawa S. (2010) RPK2 is an essential receptor-like kinase that transmits the CLV3
636 signal in Arabidopsis. *Development* 137: 3911-3920
637 Kitagawa M, Jackson D (2019) Control of Meristem Size. *Annu Rev Plant Biol* 70: 269-291
638 Lammens T, Boudolf V, Kheibarshekan L, Zalmas LP, Gaamouche T, Maes S, Vanstraelen M,
639 Kondorosi E, La Thangue NB, Govaerts W *et al* (2008) Atypical E2F activity restrains
640 APC/CCCS52A2 function obligatory for endocycle onset. *Proc Natl Acad Sci U S A* 105: 14721-
641 14726
642 Liu D, Kumar R, Claus LAN, Johnson AJ, Siao W, Vanhoutte I, Wang P, Bender KW, Yperman

643 K, Martins S *et al* (2020) Endocytosis of BRASSINOSTEROID INSENSITIVE1 Is Partly Driven
644 by a Canonical Tyr-Based Motif. *Plant Cell* 32: 3598-3612

645 Mbengue M BG, Gervasi F, Beck M, Zhou J, Spallek T, Bartels S, Boller T, Ueda T, Kuhn H,
646 Robatzek S (2016) Clathrin-dependent endocytosis is required for immunity mediated by pattern
647 recognition receptor kinases. *Proc Natl Acad Sci USA* 113: 11034-11039

648 Meijering E, Jacob M, Sarria JC, Steiner P, Hirling H, Unser M (2004) Design and validation of a
649 tool for neurite tracing and analysis in fluorescence microscopy images. *Cytometry A* 58: 167-
650 176

651 Mishev K, Lu Q, Denoo B, Peurois F, Dejonghe W, Hullaert J, De Rycke R, Boeren S, Bretou M,
652 De Munck S *et al* (2018) Nonselective Chemical Inhibition of Sec7 Domain-Containing ARF
653 GTPase Exchange Factors. *Plant Cell* 30: 2573-2593

654 Nimchuk ZL (2017) CLAVATA1 controls distinct signaling outputs that buffer shoot stem cell
655 proliferation through a two-step transcriptional compensation loop. *PLoS Genet* 13: e1006681

656 Nimchuk ZL, Tarr PT, Ohno C, Qu X, Meyerowitz EM (2011) Plant stem cell signaling involves
657 ligand-dependent trafficking of the CLAVATA1 receptor kinase. *Curr Biol* 21: 345-352

658 Nimchuk ZL, Zhou Y, Tarr PT, Peterson BA, Meyerowitz EM (2015) Plant stem cell maintenance
659 by transcriptional cross-regulation of related receptor kinases. *Development* 142: 1043-1049

660 Ogawa M, Shinohara H, Sakagami Y, Matsubayashi Y (2008) Arabidopsis CLV3 peptide directly
661 binds CLV1 ectodomain. *Science* 319: 294

662 Olsson V, Joos L, Zhu S, Gevaert K, Butenko MA, De Smet I (2019) Look Closely, the Beautiful
663 May Be Small: Precursor-Derived Peptides in Plants. *Annu Rev Plant Biol* 70: 153-186

664 Ortiz-Morea FA, Savatin DV, Dejonghe W, Kumar R, Luo Y, Adamowski M, Van den Begin J,
665 Dressano K, Pereira de Oliveira G, Zhao X *et al* (2016) Danger-associated peptide signaling in
666 Arabidopsis requires clathrin. *Proc Natl Acad Sci U S A* 113: 11028-11033

667 Paez Valencia J, Goodman K, Otegui MS (2016) Endocytosis and Endosomal Trafficking in
668 Plants. *Annu Rev Plant Biol* 67: 309-335

669 Poncini L, Wyrsh I, Denervaud Tendon V, Vorley T, Boller T, Geldner N, Metraux JP, Lehmann
670 S (2017) In roots of Arabidopsis thaliana, the damage-associated molecular pattern AtPep1 is a
671 stronger elicitor of immune signalling than flg22 or the chitin heptamer. *PLoS ONE* 12: e0185808

672 Roberts I, Smith S, Stes E, De Rybel B, Staes A, van de Cotte B, Njo MF, Dedeyne L, Demol H,
673 Lavenus J *et al* (2016) CEP5 and XIP1/CEPR1 regulate lateral root initiation in Arabidopsis. *J*
674 *Exp Bot* 67: 4889-4899

675 Schlegel J, Denay G, Wink R, Pinto KG, Stahl Y, Schmid J, Blumke P, Simon RG (2021) Control
676 of Arabidopsis shoot stem cell homeostasis by two antagonistic CLE peptide signalling pathways.
677 *eLife* 10: e70934

678 Schoof H, Lenhard M, Haecker A, Mayer KF, Jurgens G, Laux T (2000) The stem cell population
679 of Arabidopsis shoot meristems is maintained by a regulatory loop between the CLAVATA and
680 WUSCHEL genes. *Cell* 100: 635-644

681 Shinohara H, Matsubayashi Y (2015) Reevaluation of the CLV3-receptor interaction in the shoot
682 apical meristem: dissection of the CLV3 signaling pathway from a direct ligand-binding point of
683 view. *Plant J* 82: 328-336

684 Somssich M, Ma Q, Weidtkamp-Peters S, Stahl Y, Felekyan S, Bleckmann A, Seidel CA, Simon
685 R (2015) Real-time dynamics of peptide ligand-dependent receptor complex formation in planta.
686 *Sci Signal* 8: ra76

687 Stahl Y, Grabowski S, Bleckmann A, Kuhnemuth R, Weidtkamp-Peters S, Pinto KG, Kirschner
688 GK, Schmid JB, Wink RH, Hulsewede A *et al* (2013) Moderation of Arabidopsis root stemness
689 by CLAVATA1 and ARABIDOPSIS CRINKLY4 receptor kinase complexes. *Curr Biol* 23: 362-
690 371

691 Stahl Y, Wink RH, Ingram GC, Simon R (2009) A signaling module controlling the stem cell
692 niche in Arabidopsis root meristems. *Curr Biol* 19: 909-914

693 Su YH, Zhao XY, Liu YB, Zhang CL, O'Neill SD, Zhang XS (2009) Auxin-induced WUS
694 expression is essential for embryonic stem cell renewal during somatic embryogenesis in
695 Arabidopsis. *Plant J* 59: 448-460

696 Van Damme D, Coutuer S, De Rycke R, Bouget FY, Inze D, Geelen D (2006) Somatic
697 cytokinesis and pollen maturation in Arabidopsis depend on TPLATE, which has domains similar
698 to coat proteins. *Plant Cell* 18: 3502-3518

699 Van Leene J, Eeckhout D, Cannoot B, De Winne N, Persiau G, Van De Slijke E, Vercruyse L,
700 Dedecker M, Verkest A, Vandepoele K *et al* (2015) An improved toolbox to unravel the plant
701 cellular machinery by tandem affinity purification of Arabidopsis protein complexes. *Nat Protoc*

702 10: 169-187
703 Wang J, Mylly E, Johnson A, Besbrugge N, De Jaeger G, Friml J, Pleskot R, Van Damme D
704 (2020) High Temporal Resolution Reveals Simultaneous Plasma Membrane Recruitment of
705 TPLATE Complex Subunits. *Plant Physiol* 183: 986-997
706 Wang J, Yperman K, Gronos P, Jiang Q, Dragwidge J, Mylly E, Mor E, Nolf J, Eeckhout D, De
707 Jaeger G *et al* (2021) Conditional destabilization of the TPLATE complex impairs endocytic
708 internalization. *Proc Natl Acad Sci U S A* 118: e2023456118
709 Wang P, Pleskot R, Zang J, Winkler J, Wang J, Yperman K, Zhang T, Wang K, Gong J, Guan Y
710 *et al* (2019) Plant AtEH/Pan1 proteins drive autophagosome formation at ER-PM contact sites
711 with actin and endocytic machinery. *Nat Commun* 10: 5132
712 Yamaguchi YL, Ishida T, Sawa S (2016) CLE peptides and their signaling pathways in plant
713 development. *J Exp Bot* 67: 4813-4826
714 Yperman K, Papageorgiou AC, Merceron R, De Munck S, Bloch Y, Eeckhout D, Jiang Q, Tack P,
715 Grigoryan R, Evangelidis T *et al* (2021a) Distinct EH domains of the endocytic TPLATE complex
716 confer lipid and protein binding. *Nat Commun* 12: 3050
717 Yperman K, Wang J, Eeckhout D, Winkler J, Vu LD, Vandorpe M, Gronos P, Mylly E, Kraus M,
718 Merceron R *et al* (2021b) Molecular architecture of the endocytic TPLATE complex. *Sci Adv* 7:
719 eabe7999
720 Zhang Y, Persson S, Hirst J, Robinson MS, van Damme D, Sanchez-Rodriguez C (2015)
721 Change your TPLATE, change your fate: plant CME and beyond. *Trends Plant Sci* 20: 41-48

722

723 **Figure legends**

724 **Figure 1. Impaired TPC-dependent endocytic capacity confers hypersensitivity to CLV3 and CLE40** 725 **peptides.**

726 (A-B) Representative images and quantification of the root growth ratios of TPLATE_1 and WDXM2_1
727 seedlings (see Table EV1 for the specifications of the lines) treated with or without (Con) low doses of
728 CLV3 or CLE40 peptides.

729 (C-D) Representative images and quantification of the root growth ratios of TPLATE_1 and WDXM2_1
730 seedlings treated with or without (Con) different doses of FLG22, CEP5 and AtPEP1 peptides.

731 Data information: 5-day-old seedlings grown vertically on ½ MS medium plate were transferred to freshly
732 prepared ½ MS medium plates supplemented with or without low doses of peptides and grown vertically for
733 an extra 5 days. For each individual root, the primary root length after the transfer was divided by the root
734 length of the seedling before the transfer. In (B) and (D), the numbers at the bottom of the box plot and jitter
735 box graphs represent the number of individual roots measured. The box plot extends from the 25th to 75th
736 percentiles. The line inside the box marks the median. The whiskers go down and up to the 95% percentile.
737 The red dots mark the average. Differences as compared to TPLATE rescued lines are indicated (selected
738 pairs from Welch's ANOVA post hoc pairwise comparison with the Tukey contrasts); N.S., no significant
739 difference; *P < 0.05; **P < 0.01; ***P < 0.001. The data represented results from at least 4 sets of
740 seedlings grown on separate plates. Scale bar in (A) and (C) = 1cm.

741

742 **Figure 2. Impaired TPC-dependent endocytic capacity confers hypersensitivity to CLV3 in SAM.**

743 (A) Phenotypic comparison of 3- to 4-week-old TPLATE_1 and WDXM2_1 rosette stage plants grown on ½
744 MS with or without different doses of CLV3 peptide. Magenta arrows indicate terminated SAMs. Scale bar
745 = 1cm.

746 (B) Quantification of the amount of terminated shoot apical meristems in relation to the dose of CLV3
747 applied. The number of plants used for the quantification is indicated at the top of the bar chart.

748 (C-D) Representative images (C) and quantification (D) of *WUS::GUS* expression in the vegetative SAMs
749 of 3-day-old TPLATE_1 and WDXM2_1 seedlings treated with or without different doses of CLV3 peptide.
750 Intermediate (blue arrowhead) and weak (cyan arrowhead) *WUS* expression is indicated in the SAMs of
751 WDXM2_1 seedlings after CLV3 treatment. Scale bar = 50 μ m. *WUS* expression after CLV3 treatment was
752 visually scored and quantified. The numbers of seedlings analyzed is indicated at the top of the bar chart.

753 Data information: The data represented in panel B results from at least 5 sets of seedlings grown on
754 separate plates. The data represented in panel D is the combination of two independent repetitions.

755

756 **Figure 3. CLV1 loss-of-function dampens CLV3 hypersensitivity in the SAMs of WDXM2 rescued**
757 **plants.**

758 (A) Phenotypic comparisons of 3 to 4 -week-old TPLATE_1 and WDXM2_1 plants as well as combinations
759 of these with the *clv1* null (*clv1-101*) or dominant negative (*clv1-8*) mutant backgrounds under control
760 conditions or in the presence of 100 nM exogenous CLV3 peptide. The magenta arrowhead indicates a
761 terminated SAM. Scale bar = 1cm.

762 (B) Quantification of the amount of terminated meristems in relation to the dose of CLV3 peptide applied.
763 Numbers of plants used for quantification are indicated at the top of the bar chart.

764 (C) Box plot and jitter box representation of the quantification of the number of leaves produced by WDXM2,
765 WDXM2/*clv1-101* and WDXM2/*clv1-8* plants grown *in vitro* on medium supplemented with 100nM CLV3.
766 Numbers of biological samples are indicated at the bottom of the box plot and jitter box graphs. The box
767 plot extends from the 25th to 75th percentiles. The line inside the box marks the median. The whiskers go
768 down and up to the 95% percentile. The red dots mark the average. Letters (a, b and c) represent
769 significantly different groups ($P < 0.001$) evaluated by Welch's ANOVA post hoc pairwise comparison with
770 the Tukey contrasts.

771 Data information: the data represented in panel B results from at least 6 sets of seedlings grown on
772 separate plates. The data in panel C is based on a random selection of 3 to 4 plates from panel B.

773

774 **Figure 4. Reduced TPC-dependent endocytic capacity impairs internalization of CLV1 from the PM**
775 **in SAM cells.**

776 Confocal images and quantification of Arabidopsis seedlings showing enhanced PM localization of CLV1-
777 GFP in WDXM2_3 vegetative meristems compared to vegetative meristems of TPLATE_3 lines with or
778 without exogenous CLV3 (100 nM) in the growing medium from germination onward. Left panels are
779 merged channels (GFP and PI), right panels are GFP-only channels represented via an intensity scale.
780 Scale bar = 20 μ m. The Box plot and jitter box representation graph shows the average fluorescence
781 intensity (8-bit gray values) of CLV1 over the entire SAM (indicated by a dotted line). The box plot extends
782 from the 25th to 75th percentiles. The line inside the box marks the median. The whiskers go down and up
783 to the 95% percentile. The red dots mark the average. Numbers of biological samples from two repeats are

784 indicated at the bottom of the box plot and jitter box graphs. Differences of CLV1-GFP intensity between
785 WDXM2_3 and TPLATE_3 lines under both conditions were evaluated by Welch's ANOVA post hoc
786 pairwise comparison with the Tukey contrasts. Letters (a, b and c) represent significant difference between
787 groups (a,b,c; $P < 0.001$). The quantification is a combination of two independent experiments for each
788 genotype and treatment.

789

790 **Figure 5. TPC interacts with CLV1 through its AtEH1/Pan1 subunit.**

791 (A) Co-immunoprecipitation experiment comparing WT (Col-0) Arabidopsis seedlings and seedlings
792 expressing pCLV1::CLV1-2xGFP (CLV1) and 35S::eGFP (GFP). CLV1 specifically co-purifies with
793 endogenous TPLATE. The blue arrow marks full length CLV1 and the magenta arrow marks full length
794 TPLATE. Numbers next to the ladder represents the protein molecular weight (kDa). The experiment was
795 independently performed twice with an identical result. (B-C) Representative confocal images and
796 quantification of ratiometric BiFC analyses exploring the interaction between TPC subunits TPLATE, TML
797 and AtEH1/Pan1, the AP-2 complex subunit AP2M, and CLV1. The identified interaction between CLV1
798 and AtEH1/Pan1 was also performed in the presence of exogenous CLV3 peptide application (1 μM in
799 infiltration buffer). CC and NC refer to the orientation of the nYFP and cYFP halves of YFP fused to both
800 proteins. CLV1 was always tagged C-terminally. Left panels in (C) represent the YFP channel, shown via
801 an intensity scale whereas the right panels represent the RFP control channel (free RFP, magenta) against
802 which the intensity of the YFP BiFC channel was normalized. Scale bars = 25 μm . (C) Box plot and jitter
803 box representation showing the quantification of the YFP/RFP fluorescence ratios from two independent
804 experiments. The box plot extends from the 25th to 75th percentiles. The line inside the box marks the
805 median. The whiskers go down and up to the 95% percentile. The red dots mark the average. Numbers of
806 biological samples from at least two independent transformations are indicated at the bottom of the graph.
807 Letters (a, b and c) represent significantly different groups ($P < 0.001$) evaluated by Welch's ANOVA post
808 hoc pairwise comparison with the Tukey contrasts.

809 (D-E) Yeast two hybrid analysis (D) and respective quantification (E) between the cytoplasmic part of CLV1
810 (AA 671-980) and the N-terminal part of AtEH1/Pan1, which ends after the second EH domain (AA 1-527).
811 Combining CLV1 in pGADT7 (AD) with AtEH1/Pan1 in pGBKT7 (BD) allowed growth on selective medium
812 (-L-T-H; strong in 12/24 and weak in 1/24 independent double transformations) whereas only 2/24
813 transformations showed strong and 2/24 showed weak growth on selective medium in the controls, likely
814 caused by some level of auto-activation of AtEH1/Pan1. The negative control consisted of both empty
815 pGBKT7 and pGADT7 vectors (8 independent double transformations) and the positive control (eight
816 independent double transformations) combined pGADT7-SV40 T-Ag with pGBKT7-p53. No: no growth
817 observed on -L-T-H. The data shown represents individual double transformants and the assay was
818 technically repeated twice.

819

820 **Expanded View figures**

821

822 **Figure EV1. Impaired TPC-dependent endocytic capacity confers hypersensitivity to a subset of**

823 **CLE peptides.**

824 (A-B) Representative images and quantification as box plot and jitter box graphs of the root growth
825 between TPLATE_1 and WDXM2_1 seedlings grown for 8 days in the presence or absence of low doses
826 (10 nM) of different CLE peptides. Scale bar = 1cm. Primary root growth was quantified for a number of
827 seedlings ($16 \leq N \leq 28$) and statistically significant differences were observed for CLE10, CLV3 and CLE40.
828 ***, $P < 0.001$ (selected pairs from Welch's ANOVA post hoc pairwise comparison with the Tukey contrasts).
829 N.S., no significant difference. The experiment was performed twice with a similar outcome. The box plots
830 extend from the 25th to 75th percentiles. The line inside the box marks the median. The whiskers go down
831 and up to the 95% percentile. The red dots mark the average. The dots represent measurements of
832 individual seedlings. The data represented is the quantification of one experiment where at least 3 sets of
833 seedlings were grown on separate plates.

834

835 **Figure EV2. The weak TPC subunit mutant allele *twd40-2-3* confirms the observed CLV3 and CLE40**
836 **hypersensitivity in the WDXM2_1 line.**

837 (A-B) Representative images (A) and comparison (B) of the primary root growth ratios between TPLATE_1,
838 WDXM2_1 and *twd40-2-3* seedlings transferred to plates with or without 10 nM CLV3 or CLE40. Root
839 growth for each root after transfer was divided by the root length before transfer. Numbers of seedlings
840 used for the quantification are indicated at the bottom of the box plot and jitter box graphs. The box plots
841 extend from the 25th to 75th percentiles. The line inside the box marks the median. The whiskers go down
842 and up to the 95% percentile. The red dots mark the average. The dots represent measurements of
843 individual seedlings. Scale bar = 1cm.

844 Data information: in panel (B): Differences as compared to TPLATE rescued lines were evaluated by
845 Welch's ANOVA post hoc pairwise comparison with the Tukey contrasts. Letters (a, b and c) represent
846 significant difference between groups ($P < 0.001$). The quantification represented results from at least 5
847 sets of seedlings grown on separate plates.

848

849 **Figure EV3. Impaired TPC-dependent endocytic capacity confers CLV3 hypersensitivity in the SAM**
850 **and this hypersensitivity correlates with the expression level of the complementing construct.**

851 (A) Phenotypic comparison of 3 to 4 -week-old independent TPLATE (TPLATE_1 and TPLATE_3) and
852 WDXM2 (WDXM2_1 and WDXM2_3) lines (GFP and mSCARLET fusions respectively) grown in the
853 presence or absence of CLV3 peptide. Magenta arrows indicate terminated SAMs. Scale bars = 1 cm.

854 (B) Quantification of the number of plants with a terminated meristem induced by the CLV3 peptide. The
855 numbers of plants used for the quantification is indicated at the top of the bar chart. The experiment was
856 repeated twice and the quantification in panel B combines both experiments.

857 (C) Anti-TPLATE western blot detecting the presence of endogenous TPLATE in Col-0 (asterisk) as well as
858 the full length of GFP (TPLATE_1, WDXM2_1 and WDXM2_2) or mSCARLET (TPLATE_3 and WDXM2_3)
859 fusions of TPLATE and WDXM2 in the rescued *tplate(-/-)* homozygous mutant background that lacks
860 endogenous TPLATE. For an unknown reason, the mSCARLET fusions give rise to several bands on the

861 blot. The WDXM2_2 line showed a similar expression level as the WDXM2_1 and was not used further.
862 The reduced expression in WDXM2_3 correlates with an increased hypersensitivity to the CLV3 treatment.
863 The large subunit of RUBISCO (around 50 kDa) visualized via the stain free gel, was used as loading
864 control.

865

866 **Figure EV4: TPLATE and WDXM2 expression and localization in flower meristems and**
867 **internalization of CLV1.**

868 (A) Serial optical cross sections through the inflorescence meristem, showing localization of TPLATE and
869 WDXM2 in layer 1 to 3 (L1-L2-L3). Left images are intensity scaled. Images on the right for each genotype
870 represent the merged GFP and PI channels. Scale bar = 25 μ m.

871 (B) Representative Z-stack projections (3 optical slices, \sim 3 μ m) of flower meristems of TPLATE_3 and
872 WDXM2_3 lines expressing pCLV1::CLV1-GFP with or without (mock) short term exogenous CLV3
873 treatment (30 min; 100 μ M). The quantification shows the relative number of meristems with strong or weak
874 vacuolar accumulation of CLV1. n = 8 for TPLATE_3(mock); n = 8 for TPLATE_3(CLV3); n = 4 for
875 WDXM2_3(mock) and n = 6 for WDXM2_3(CLV3). Scale bar = 20 μ m.

876 (C) Western blots showing the bead fraction of two independent IP experiments of CLV1 from flower
877 meristems of TPLATE_3 and WDXM2_3 lines with (+) or without (-) short term treatment with exogenous
878 CLV3 (30 min; 100 μ M). The quantification shows the fraction of the free GFP degradation band at 25kDa
879 over the total amount of signal. The line presents the mean and the dots represent the results of the two
880 independent experiments. MW = molecular weight marker (kDa).

881

882 **Figure EV5. Reduced TPC-dependent endocytic capacity impairs internalization of CLV1 from PM in**
883 **vegetative SAM cells upon short-term CLV3 treatment.**

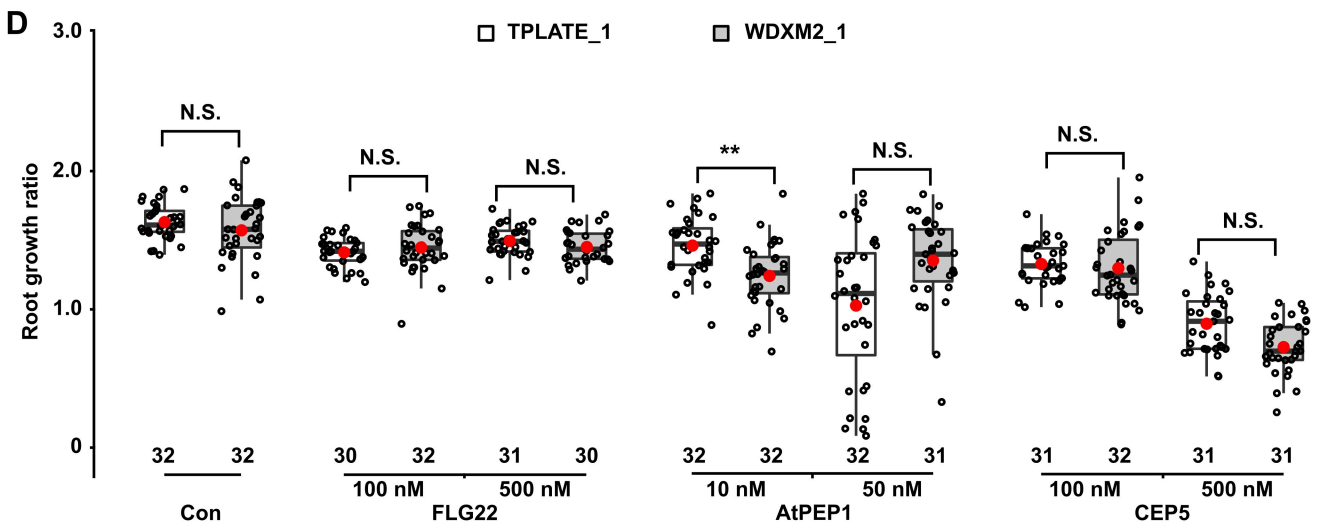
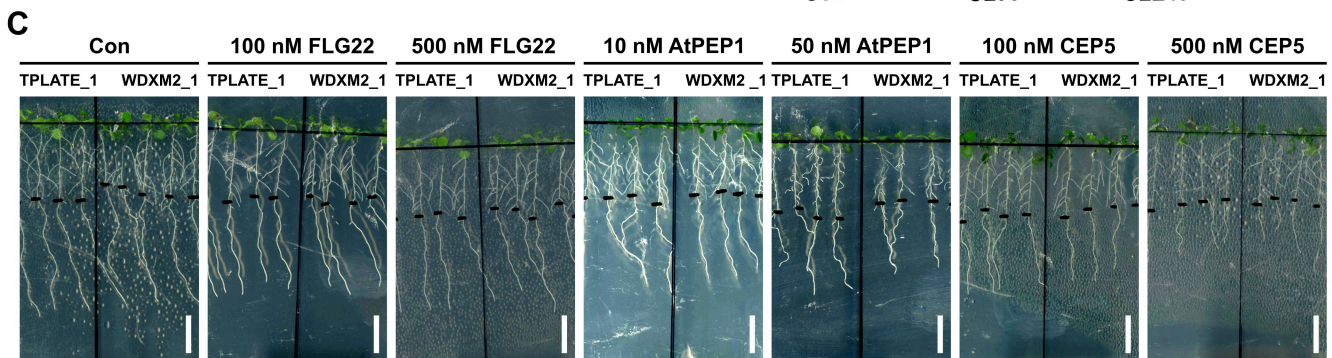
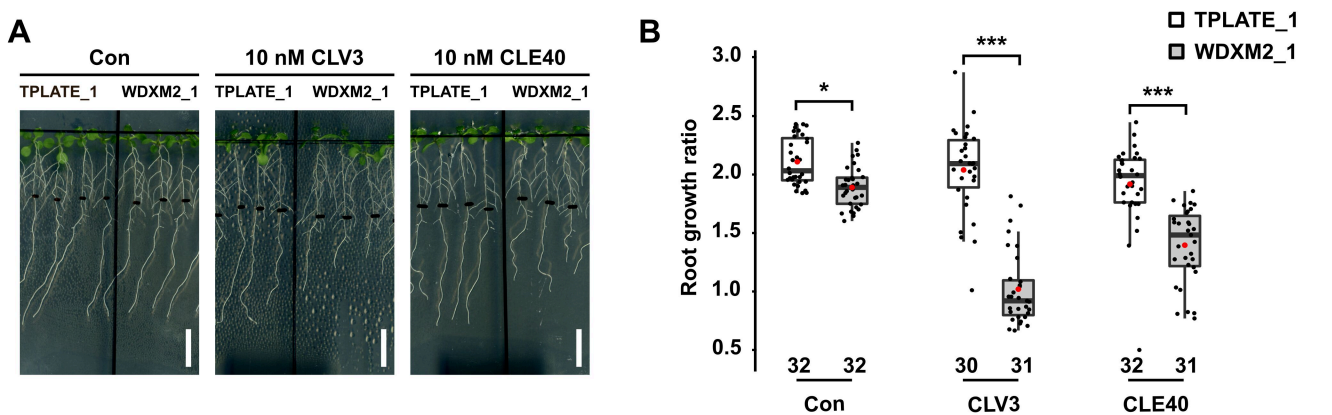
884 (A) Representative images of two vegetative SAMs in the TPLATE_3 background, with different levels of
885 CLV1 expression, imaged before and after exogenous CLV3 treatment (1 μ M for 30 min). Two different
886 focal planes of a Z-stack, visualizing different L3 cells per SAM are represented for each timepoint. For
887 both SAMs, the CLV1 intensity at PM reduces upon CLV3 treatment.

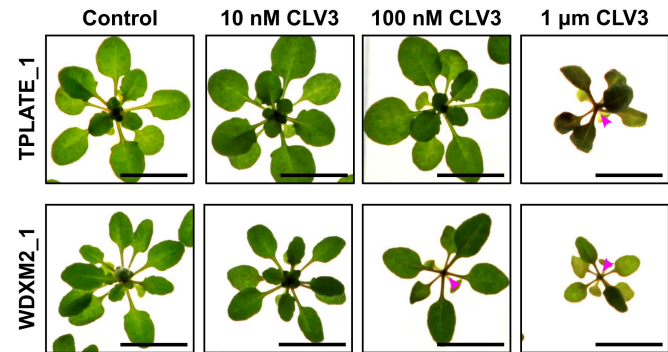
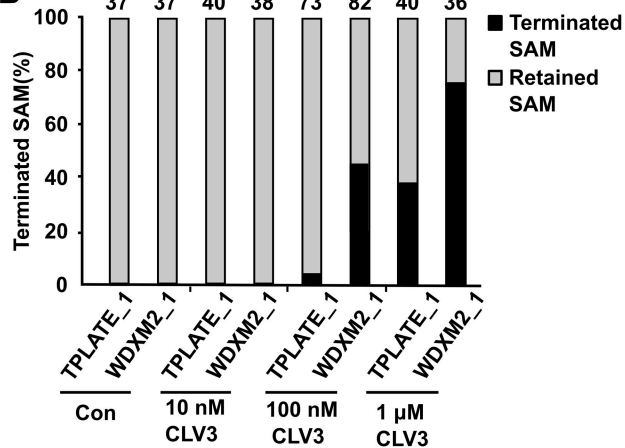
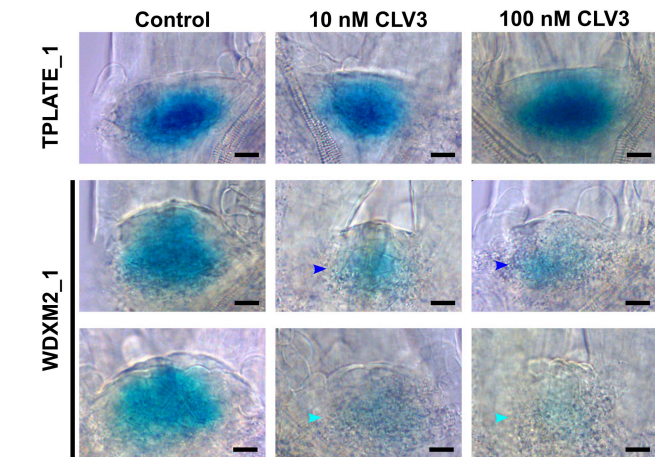
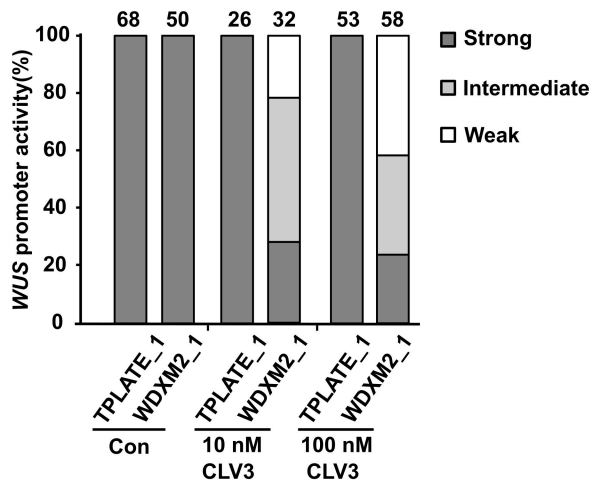
888 (B-E) Representative confocal images and quantification of Arabidopsis TPLATE_3 and WDXM2_3
889 expressing seedlings following short-term CLV3 peptide treatment (1 μ M for 10 min: B-C and 1 μ M for 30
890 min: D-E). Similar to the long-term treatment (Fig 4), PM localization of CLV1-GFP reduces upon CLV3
891 peptide treatment, which is not the case in WDXM2_3 vegetative meristems. The box plot and jitter box
892 representation graph represents the average fluorescence intensity (8-bit gray values) of CLV1 over the
893 entire SAM (indicated by a dotted line). Numbers of biological samples from two repeats are indicated at
894 the bottom of the box plot and jitter box graphs. The box plots extend from the 25th to 75th percentiles. The
895 line inside the box marks the median. The whiskers go down and up to the 95% percentile. The red dots
896 mark the average. The dots represent measurements of individual seedlings. Differences of CLV1-GFP
897 intensity between WDXM2_3 and TPLATE_3 lines under both conditions were evaluated by Welch's
898 ANOVA post hoc pairwise comparison with the Tukey contrasts. Letters (a, b and c) represent significant
899 difference between groups (a and b, $P < 0.001$; b and c, $P < 0.05$). The quantification combines at least two
900 independent experiments for each genotype, treatment and duration of treatment. Left panels are merged

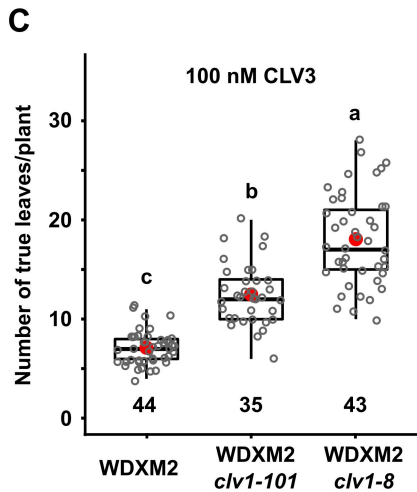
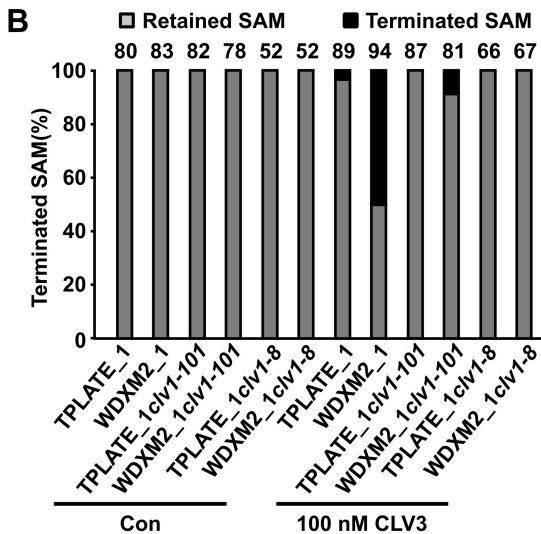
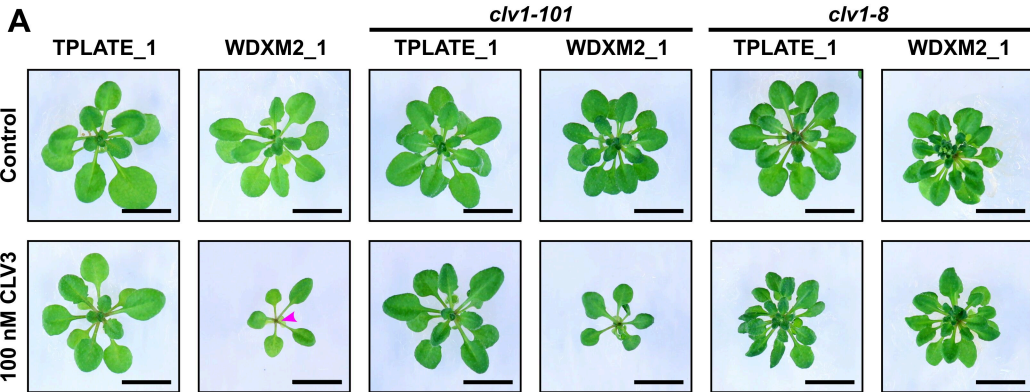
901 channels (GFP and PI), right panels are GFP-only channels represented via an intensity scale. Scale bar in
902 (A), (B) and (D) = 20 μm .

903

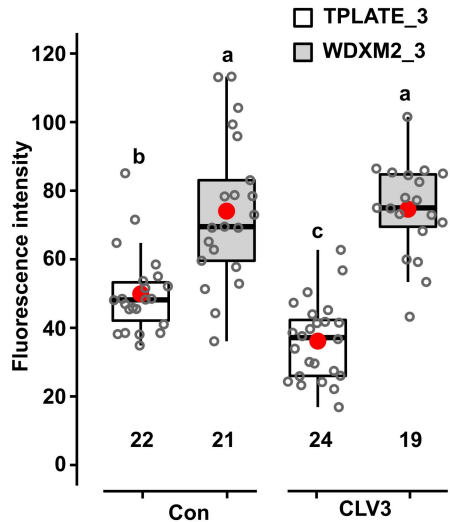
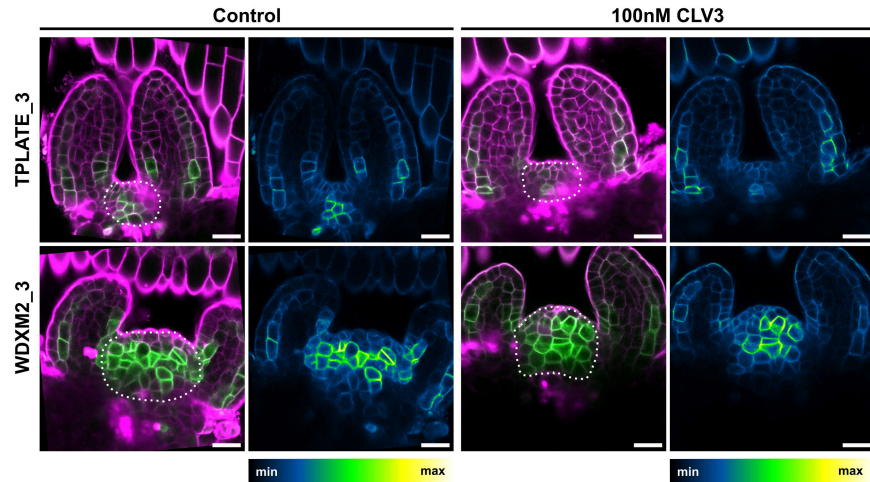
904

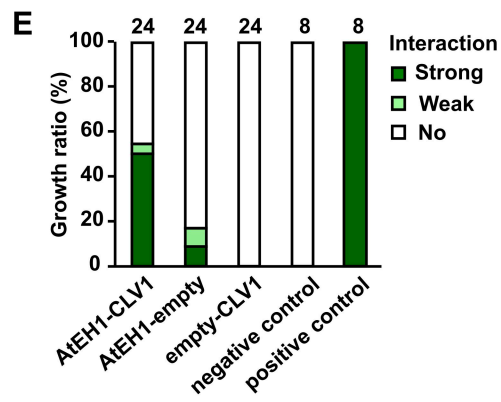
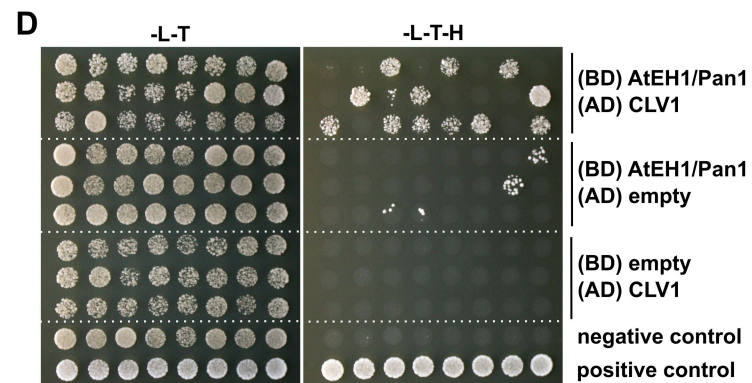
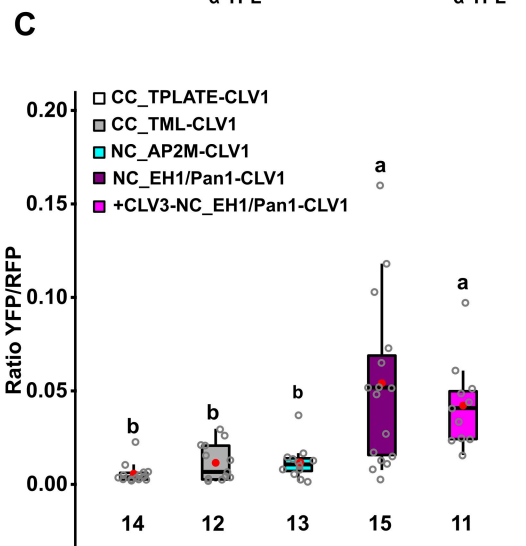
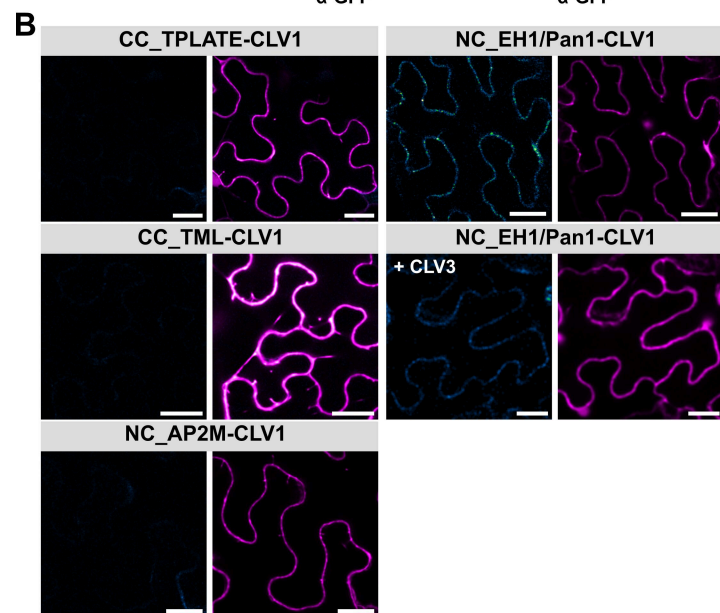
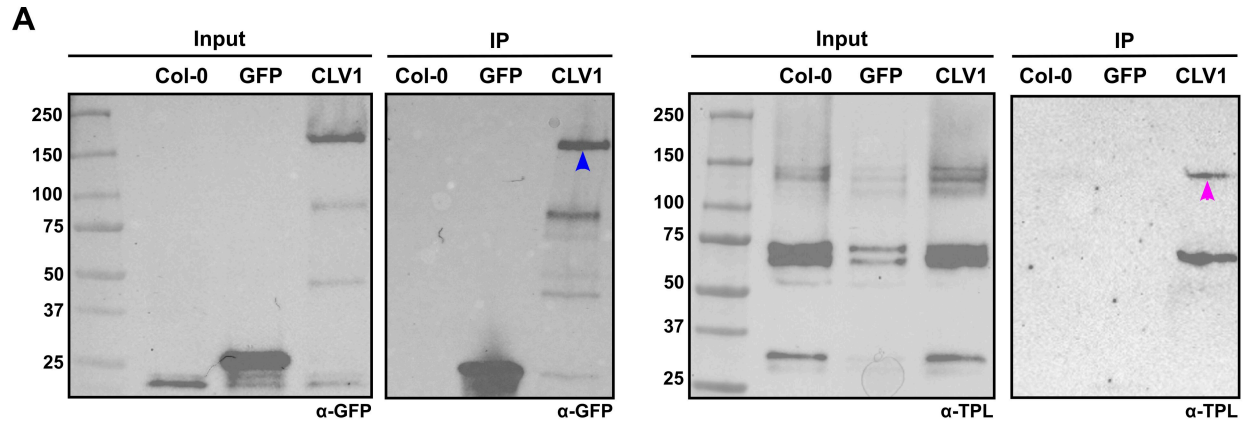


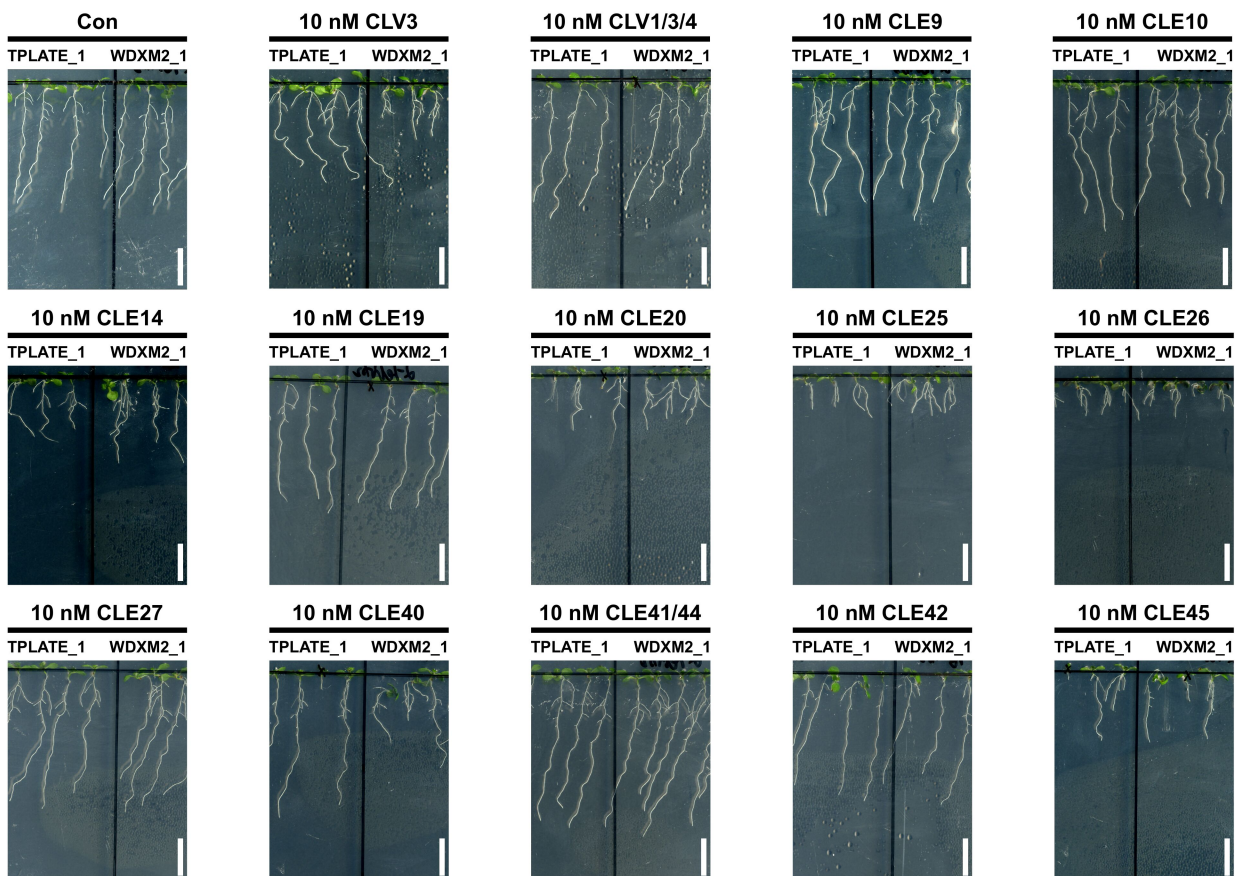
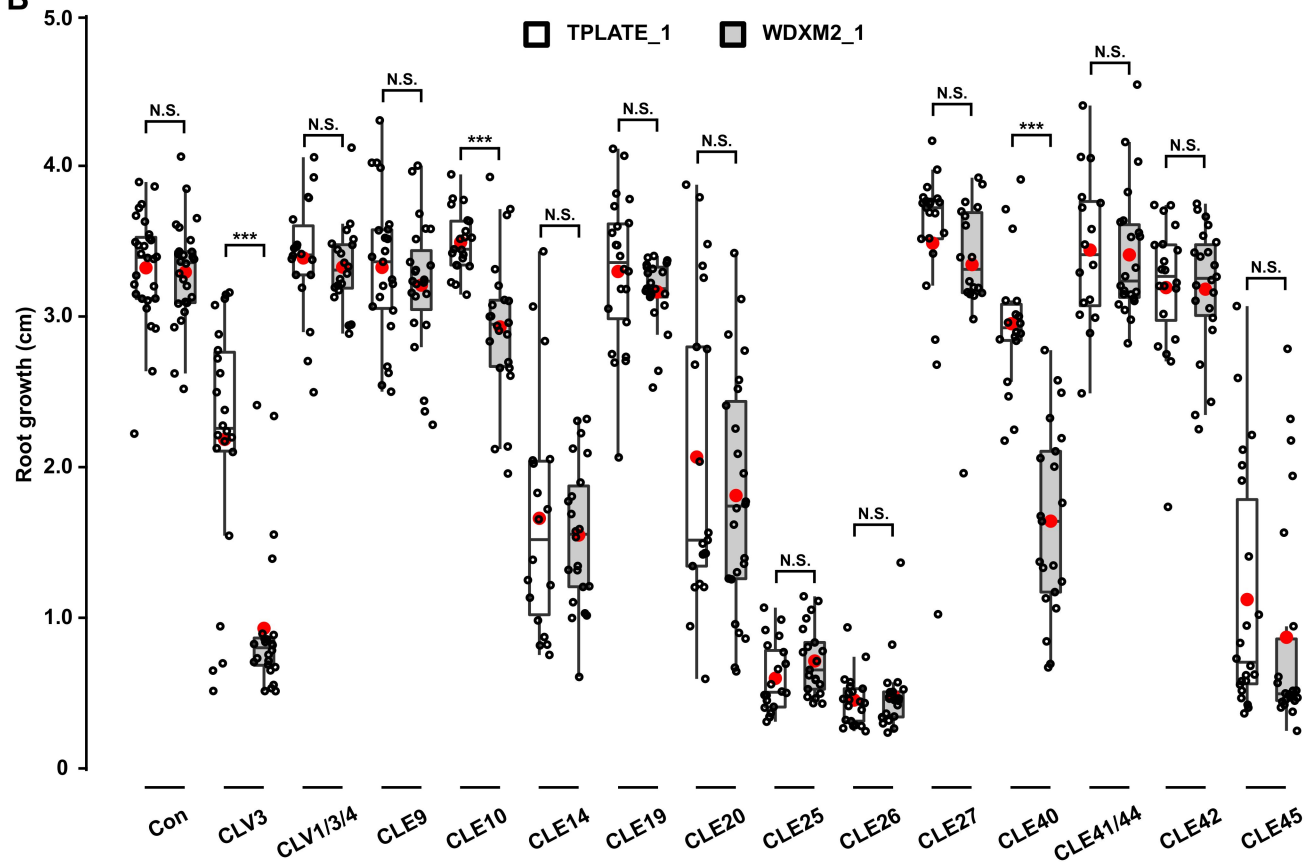
A**B****C****D**

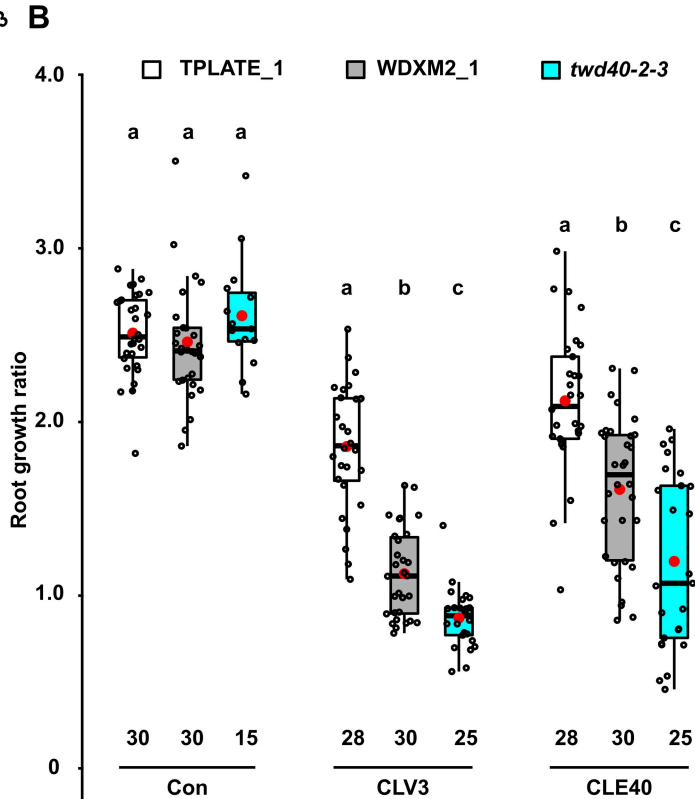
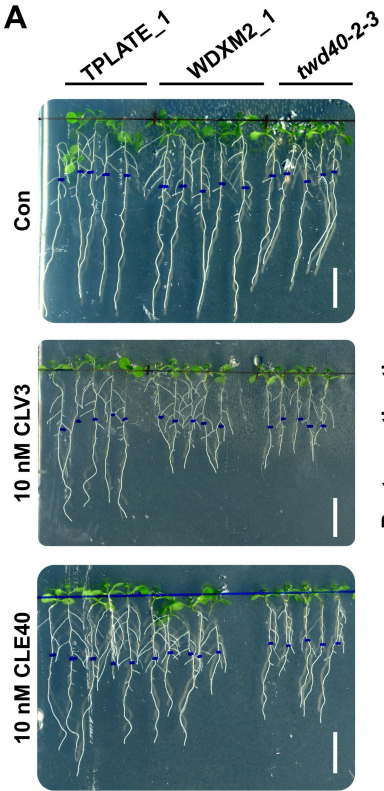


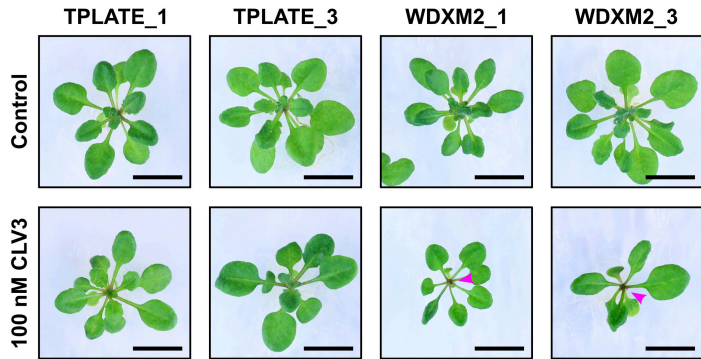
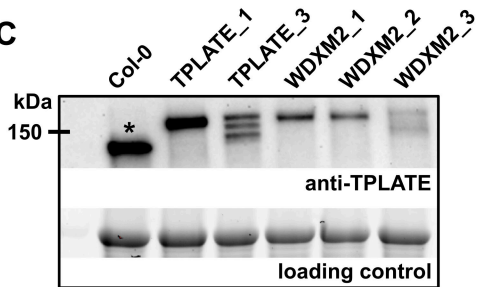
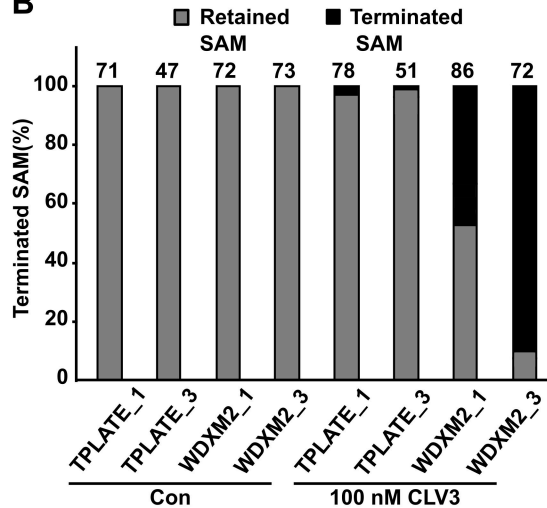
pCLV1:CLV1-GFP + PI

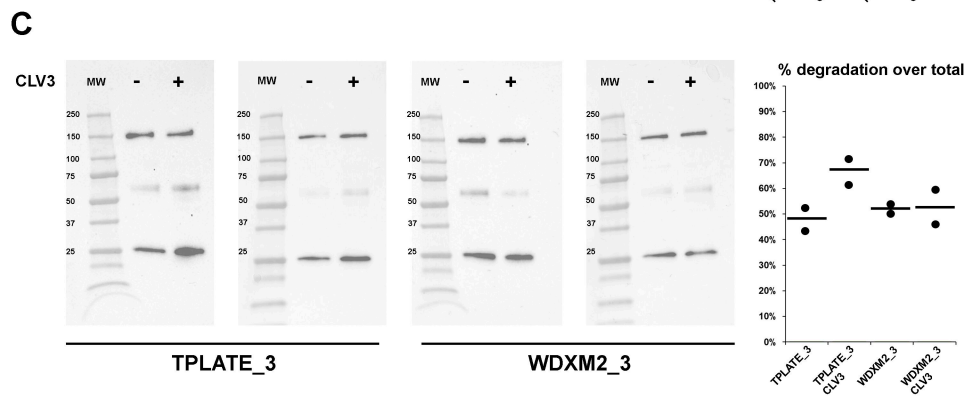
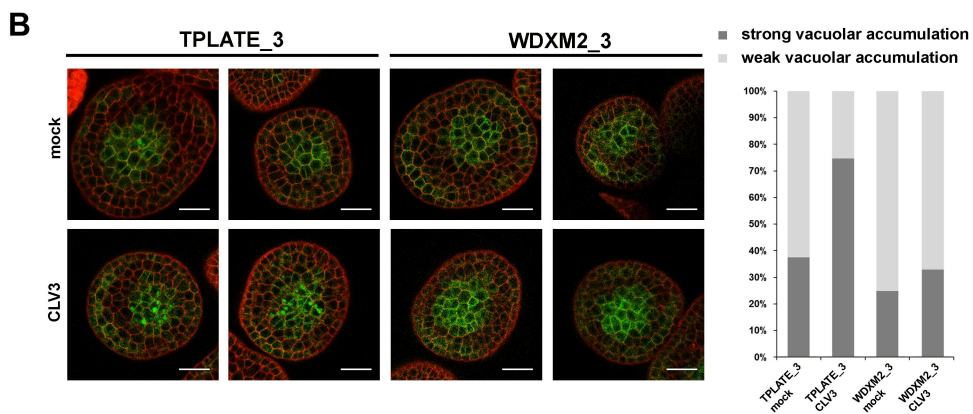
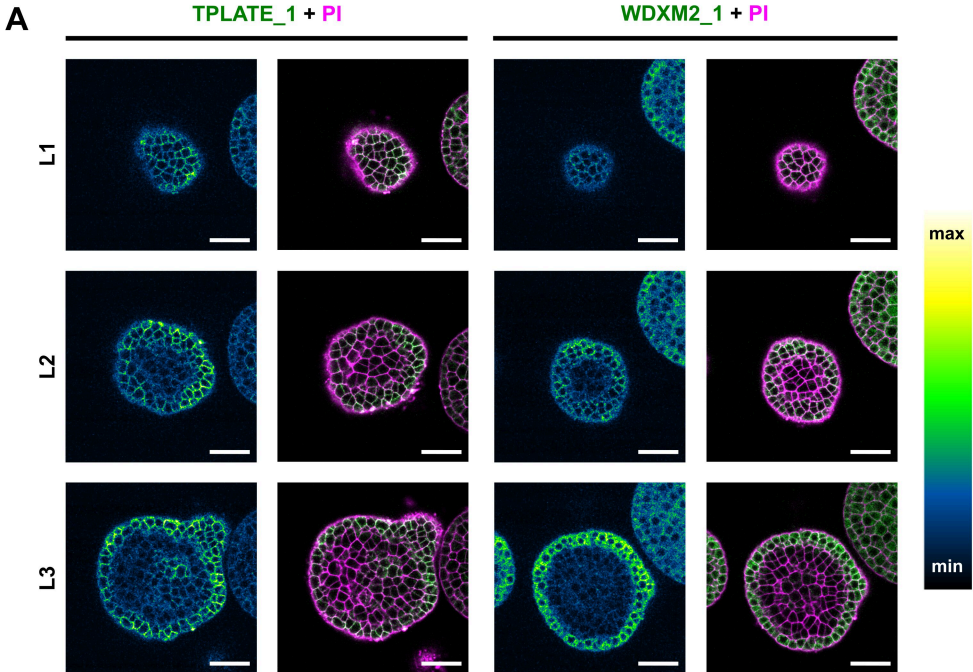


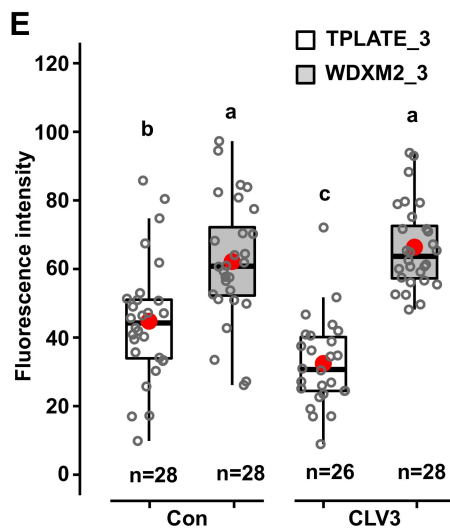
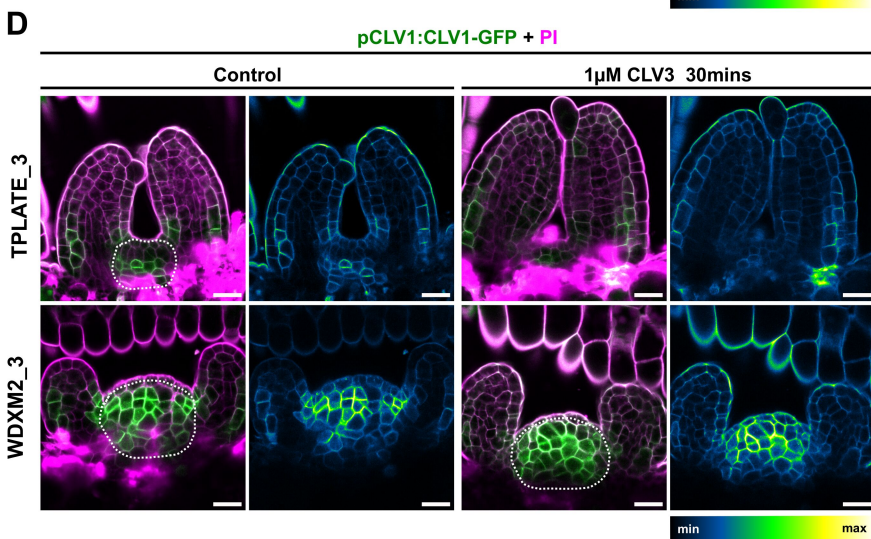
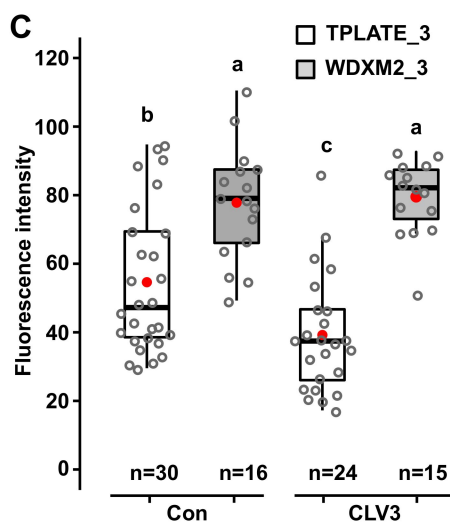
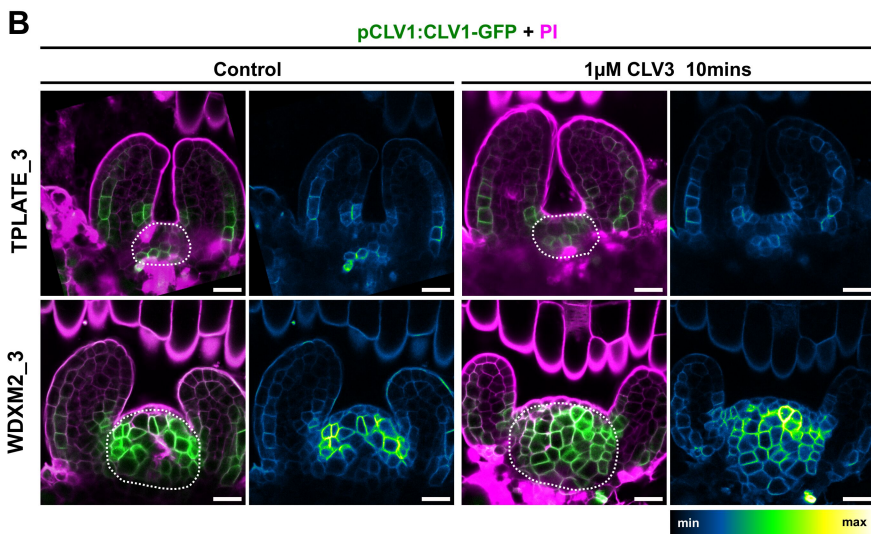
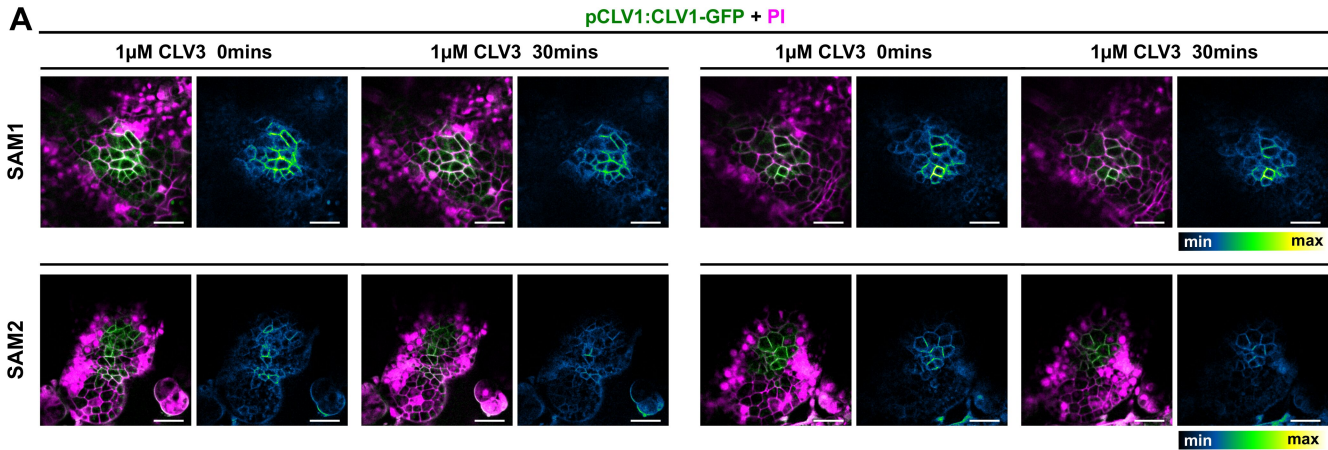


A**B**



A**C****B**





Plant lines	Full name	Background	Antibiotic selection	Identification	Resources
<i>tplate</i>		(+/-) (+/+)		GPCR	Van Damme et al., 2006
<i>twd40-2-3</i>		(-/-)		GPCR	Bashline et al., 2015
TPLATE_1	pLAT52-TPLATE-GFP	<i>tplate</i> (-/-)	H	GPCR	Van Damme et al., 2006
TPLATE_3	pLAT52-TPLATE-mScarlet	<i>tplate</i> (-/-)	H	GPCR	This study
WDXM2_1	pLAT52-WDXM2-GFP	<i>tplate</i> (-/-)	B	GPCR	Wang et al., 2021
WDXM2_2	pLAT52-WDXM2-GFP	<i>tplate</i> (-/-)	B	GPCR	Wang et al., 2021
WDXM2_3	pLAT52-WDXM2-mScarlet	<i>tplate</i> (-/-)	H	GPCR	This study
<i>clv1-101</i>		(-/-)			Kinoshita et al, 2010
<i>clv1-8</i>		(-/-)			Dievart et al., 2003
TPLATE_1 <i>clv1-101</i>	pLAT52-TPLATE-GFP	<i>tplate</i> (-/-) <i>clv1-101</i> (-/-)		GPCR	This study
WDXM2_1 <i>clv1-101</i>	pLAT52-WDXM2-GFP	<i>tplate</i> (-/-) <i>clv1-101</i> (-/-)		GPCR	This study
TPLATE_1 <i>clv1-8</i>	pLAT52-TPLATE-GFP	<i>tplate</i> (-/-) <i>clv1-8</i> (-/-)		GPCR, Sequence	This study
WDXM2_1 <i>clv1-8</i>	pLAT52-WDXM2-GFP	<i>tplate</i> (-/-) <i>clv1-8</i> (-/-)		GPCR, Sequence	This study
WUS-GUS	pWUS-GUS	<i>Col_0</i>			Su et al., 2009
TPLATE_1 pWUS-GUS	pLAT52-TPLATE-GFP/pWUS-GUS	<i>tplate</i> (-/-)		GPCR, GUS staining	This study
WDXM2_1 pWUS-GUS	pLAT52-WDXM2-GFP/pWUS-GUS	<i>tplate</i> (-/-)		GPCR, GUS staining	This study
CLV1-GFP	pCLV1-CLV1-GFP	<i>Col_0</i>			Prof. Rüdiger Simon
TPLATE_3 CLV1-GFP	pLAT52-TPLATE-mScarlet/pCLV1-CLV1-GFP	<i>tplate</i> (-/-)		GPCR, Basta	This study
WDXM2_3 CLV1-GFP	pLAT52-WDXM2-mScarlet/pCLV1-CLV1-GFP	<i>tplate</i> (-/-)		GPCR, Basta	This study
eGFP	p35S-eGFP	<i>Col-0</i>			Obtained from Prof. E. Russinova

Table EV1: list of used Arabidopsis lines

The table provides an overview of the lines used, their genetic background and references.

H: Hygromycin; B: Basta; GPCR: Genotyping PCR; (-/-): homozygous mutant background;

(+/-): heterozygous mutant background.

	Name	Sequence and modifications	MW	Purity (%)	Stock solution
1	CLV3	RTVHypSG[Ara3]HypDPLHHH	1449,58	95,7	100 µM/water
2	CLE1/3/4	RLSPGGPDPRHH	1325,44	94,3	100 µM/water
3	CLE9	RLVHypSGHypNPLHN+[Ara3], [Ara4] or[Ara6]	1300,47	95	100 µM/water
4	CLE10	RLVPSGPNPLHN	1300,47	98,4	100 µM/water
5	CLE14	RLVPGKPNPLHN	1341,57	84,8	100 µM/water
6	CLE19	RVIPTGPNPLHN	1314,5	85,6	100 µM/water
7	CLE20	RKVKTGSNPLHN	1350,53	96,5	100 µM/water
8	CLE25	RKVPNGDPIHN	1340,5	94,4	100 µM/water
9	CLE26	RKVPRGPDPIHN	1385,58	91,2	100 µM/water
10	CLE27	RIVPSCPDLHN	1347,55	74,2	100 µM/water
11	CLE40	RQVPTGSDPLHH	1343,45	92,5	100 µM/water
12	CLE41/44	HEVPSGPNPISN	1247,32	89,9	100 µM/water
13	CLE42	HGVPSGPNPISN	1175,26	93,9	100 µM/water
14	CLE45	RRVRRGSDPIHN	1462,63	88,6	100 µM/water

Table EV2: Information of CLE peptides used in this research.

The table provides an overview of the sequences of the various CLE peptides used, their molecular weight (MW), purify and stock concentration. Hyp: Hydroxyproline; Ara: Arabinosylated.